Experimental Dynamic Substructuring

Coupling and Decoupling

- Application to Ampair 600 Wind Turbine -

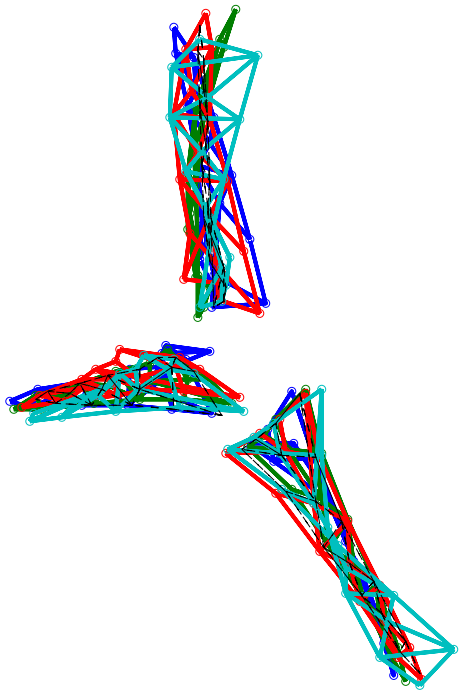

Author: Siamand Rahimi

Supervisor TU Delft: Prof. Dr. Ir. Daniel J. Rixen

Supervisor TU Delft: Dr. Ir. Dennis de Klerk

April 10, 2012

Abstract

The need to analyze and optimize the large and complex structures, locally and globally, and have knowledge of local and global dynamic, has induced the notion of Dynamic Substructuring. In the course of time several DS techniques are developed from which some are mainly based on experimental routine. They are known as experimental DS and assemble measured and analytically derived substructures in the frequency domain.

In order to advance, compare and classify the experimental DS theory and technology a test bed (Ampair 600 wind turbine) is initiated by the substructuring focus group at the Society for Experimental Mechanics. Based on this idea the Engineering Dynamic workgroup at Delft University of Technology has started his program which runs through couple of iterations before the Ampair 600 is completely analyzed.

This thesis concentrates on the first iteration in which attempt is done to combine three blades with the hub. The emphasis is on the Frequency Based Substructuring (FBS) in general and Lagrange Multiplier Frequency Based Substructuring (LM FBS) and experimental modeling techniques in specific.

First DS is introduced followed by FBS and LM FBS. The LM FBS formulation for both coupling and decoupling are given and typical difficulties associated with experimental DS such as rigid body dynamic, coordinates incompleteness (the lack of Rotational Degrees of Freedom), noise and inconsistency are underlined and some methods are proposed to tackle them or minimize their influences.

The notion of interface loading is adopted and applied using a fixture which mass loads and stiffens (rigidifies) the interface. The fixture is a chopped off version of the actual joint. As consequence the joint stiffness and damping are included in the models after removing the fixture by means of LM FBS decoupling technique.

To model the Cyclic Symmetric Structures (CSS) two methods are proposed which seems to contribute to consistent and robust experimental modeling. One produces models from measurement data and the other one lumped models. Both construct models which are defined in the local coordinates of the interface nodes.

The assembly results of four coupling variants according to LM FBS are given, validated and evaluated. It is shown that using regenerated models, particularly when the structures are too complex, results in wrong prediction of the assembled system.

The results of the best two coupling variants are more discussed in details and their eigenmodes up to $185\ Hz$ are indentified and visualized.

Acknowledgments

Nine month ago I have been given the opportunity to work on the Ampair test bed at Delft University of Technology. Before I could get to this end I have experienced up and downs and have seen how stupidity can make wise. This work is limited to what is written here and what is not written here is the most important part.

They say everything is clear before we start taking about them but it is proven to me that everything becomes clear when the thoughts are written down. At that moment they seem to lose their importance and any other things which are not there start to trigger. Hopefully this process will continue until we maybe reach the limit of our words which is the limit of our world.

Looking back the most joyful times were those when the thought were free and clear or when the reasons behind the mistakes became obvious. It was also a great pleasure to see how theory and practice could be brought together.

As they say Knowledge is in the end based on acknowledgement. So I would like to thank everyone whose has been involved in my work or has been supporting me during the whole process, unconditionally.

Many thanks go to Dr. Ir. Dennis de Klerk for his encouragement, frankness and positive attitude. His ability to bring people together and motivating them is absolutely exemplary.

I would like to express my gratitude to Prof. Dr. Ir. Daniel J. Rixen for his inspiration, willingness, passion and the way of teaching. He has taught us how to simplify systematically in order to understand and interpret.

Den Haag

April 2012

Siamand Rahimi

Content

Abstract I

Acknowledgments III

Nomenclature VII

Abbreviations VII

Symbols VII

1 Introduction 1

1.1 Thesis Assignment 2

1.2 Thesis outline 2

2 Dynamic substructuring 5

2.1 Frequency Based Substructuring 6

2.2 Lagrange Multiplier FBS 9

2.3 Decoupling using LM FBS 10

3 Inertia Properties, Rotational DoF's and noise 13

3.1 Measuring Inertia properties 15

3.2 Rotational DoF's 18

3.3 Preparing and monitoring the measurement 20

4 Cyclic Symmetric Structure 21

4.1 Coordinates transformation 22

4.2 CSS Synthesizing 23

4.3 Inertia properties and Lumped CSS model 24

5 Experimental DS Test bed 27

5.1 The Blades 29

5.2 The Brackets 31

5.3 The Hub 31

6 Substructures models 33

6.1 Blade model 35

6.2 Hub models 37

7 Assembly and Validation 43
7.1 Coupling procedure and coupling variants 45
7.2 Validation 46
7.3 Discussion 50
8 Conclusion and Recommendations 53
8.1 Conclusion 55
8.2 Recommendations 57
Bibliography 59
Appendix A 61
Appendix B 65
Appendix C 71

Nomenclature

Abbreviations

CG	Center of gravity
CMIF	Complex Mode Indicator Function
CMS	Component Mode Synthesis
CSS	Cyclic Symmetric structures
DoF	Degrees of Freedom
DS	Dynamic substructuring
FBS	Frequency Based Substructuring
FRAC	Frequency Response Assurance Criterion
FRF	Frequency Response Functions
IDM	Interface Deformation Modes
IRM	Inertia Restraint Method
LM	Lagrange Multiplier
LM FBS	Lagrange Multiplier Frequency Based Substructuring
MBL	Measured blade-lumped hub
MBF	Measured blade-full hub
ODS	Operational Deflection Shape
RDoF	Rotational Degree of Freedom
RBL	Regenerated blade-lumped hub
RBF	Regenerated blade-full hub
SEM	Society of Experimental Mechanics
TDoF	Translational Degree of Freedom

Symbols

M	mass matrix
K	stiffness matrix
F	applied force vector
g	coupling force vector
u	displacement vector
L	boolean localization matrix

B	signed boolean matrix
q	unique set of DoF's
λ	lagrange multiplexers
Z	dynamic stiffness
Y	dynamic flexibility (receptance, mobility or accelerance)
ω	angular frequency
m	total mass
t	applied torque vector
r	displacement vector relative to a given coordinate system
J	tensor of inertia
T	geometrical transformation matrix
R	transformation matrix
C	circulant matrix
α	acceleration vector
$\blacklozenge^{(S)}$	associated to substructure s
$\blacklozenge_i$	internal DoF
$\blacklozenge_c$	coupling DoF
$\tilde{\blacklozenge}$	reduced matrix/vector

1 Introduction

Complex and big structures such as wind turbines and airplanes are normally analyzed by means of Dynamic Substructuring (DS). DS implies dividing a structural system into subsystems (substructures), modeling them one by one and assembling them analytically. As a result local optimization is more feasible and more insight is going to be gained over the local dynamics of the substructures without loss of generality. Also different design groups could work independently and exchange information.

DS methods are time or frequency based. Recently Frequency Based Substructuring (FBS) has gained popularity as it uses experimentally derived (measured) Frequency Response Functions (FRF). This popularity is mainly caused by two reasons;

- first, the measured FRF's contain a considerable amount of information, and have the advantage of including all structural information, such as damping and the effect of the higher modes.
- second, nowadays testing equipments are becoming faster and faster and are more robust and more software and tools are available. Consequently modeling complex structures which costs lost of time and requires too much effort, can be realized much faster and more reliable through experimental routines.

To make advantage of these facts the DS subgroup as a part of the Society of Experimental Mechanics (SEM) is formed to advance the Experimental DS. The focus lies on studying, evaluating and advancing of different experimental dynamic modeling strategies in order to identify a generalized modeling methodology and provide guidance on the use of it. The pitfalls should be illuminated and the benefits should be optimized.

Sandia Labs has initiated the process and candidate a small 600 Ampair wind turbine to advance the focus group. As a participant in the focus group, the Engineering Dynamic

workgroup at Delft University of Technology contributes in this process and will apply its modeling technique and coupling/decoupling formulation to the chosen structure. Other organizations which are participating are; University of Massachusetts-Lowell, University of Wisconsin, University of Chalmers, University of Stuttgart, University of D'aCquila and the UK Atomic Weapon Establishment.

1.1 Thesis Assignment

This MSc thesis has been carried out at Delft University of Technology, department Precision and Micro Engineering, under the supervision of Prof. Daniel Rixen and Dr. Dennis de Klerk during a period of nine months. The objective of the assignment is:

"Apply Lagrange Multiplier Frequency Based Substructuring (Coupling/Decoupling) to the 600 Ampair wind turbine in order to accomplish the first iteration by assembling the blades with the hub"

This thesis concentrates on the substructure modeling, particularly in the cases where no analytical models of substructures exist. An Attempt is done to set up a methodology and form a theoretical framework for modeling the intended substructures through experimental routines. The objective is to minimize the noise and measurement inconsistency.

To accomplish the assignment successfully a type of structure is introduced which is known as cyclic symmetric structure. The structural properties of such a structure are then used to simplify the modeling steps.

In addition efforts are made to measure the inertia properties of a substructure using impact measurement.

The practical and theoretical relevancies of this thesis are related to the way the substructures are modeled to obtain high fidelity models from the raw measured data for coupling/decoupling purposes.

As the LM FBS has already been validated if relatively noise free and consistent models are going to be used the results are expected to be reliable

1.2 Thesis outline

This thesis can be divided into three parts. The first part discussed the theory, based on which the modeling and assembly has been performed.

First the notion of DS is discussed followed by FBS approach and different assembly

procedures. Then both coupling and decoupling formulations, given by LM FBS are dealt with. Thereafter the problems pertaining to Experimental models such as; coordinate incompleteness, rigid body modes, inertia properties, noise and inconsistency are tackled. And finally Cyclic Symmetric Structures are treated and is proposed how to model them and how to lump them.

The second part describes the Experimental DS test bed in general and specifies which substructures are going to be modeled and assembled in this work. It gives a detailed description of how the actual substructures are modeled.

In the third part the assembly results of different coupling variants are given and are validated. After validation two coupling variants are selected to be studied and evaluated more in depth. The mode shapes are extracted and visualized. This part is extended with discussion and is finished with conclusion and recommendations.

2 Dynamic substructuring

Dynamic substructuring (DS) refers to dividing a structural system into several subsystems, modeling them separately and putting them back to together analytically in order to have a whole again. It allows investigating the dynamic of structures which are too complex or to big to be analyzed as one piece. As consequence more insight can be gained over the local dynamic of the substructures and local optimization is feasible. In this process each substructure is represented with its analytical, discretized or experimental model. Depending on the domain in which the assembly is done the DS can be categorized into time-domain based and frequency domain based methods.[1]

The time-domain based methods employ physical or modal models while the frequency domain based methods use Frequency Response Functions (FRF). These domains are analytically interchangeable which make it possible to combine the analytical and experimental models in one of the desirable domains. The process in which the substructures are combined is called Coupling or Assembling. Assembling in the modal domain is known as Component Mode Synthesis (CMS) while doing that in the frequency domain is called Frequency Based Substructuring (FBS).

To couple the substructures two conditions must be met; compatibility and equilibrium. Compatibility ensures that the displacements at coupling points are equal while equilibrium equilibrates the forces at those points. The assembly can be done in a primal or dual fashion. Satisfying the compatibility prior to equilibrium yields the primal formulation whereas interchanging this sequence gives the dual formulation.

[1] A comprehensive classification of the DS techniques is given by de Klerk et al. [1].

2.1 Frequency Based Substructuring

The dynamics of a structure/substructure can be analyzed in the physical, modal or frequency domain.[1] In the physical domain the discretized structure model is represented with its mass, stiffness and damping matrix while in the modal domain a linear combination of the normal modes and their augmentations describes the structure. The physical model of n uncoupled and undamped (conservative) substructures is:

$$M\ddot{u} + Ku = F + g \tag{2.1}$$

Where,

$$M \triangleq \begin{bmatrix} M^{(1)} & \cdots & 0 \\ \vdots & \ddots & \vdots \\ 0 & \cdots & M^{(n)} \end{bmatrix} \qquad K \triangleq \begin{bmatrix} K^{(1)} & \cdots & 0 \\ \vdots & \ddots & \vdots \\ 0 & \cdots & K^{(n)} \end{bmatrix}$$

$$u \triangleq \begin{bmatrix} u^{(1)} \\ \vdots \\ u^{(n)} \end{bmatrix} \qquad f \triangleq \begin{bmatrix} F^{(1)} \\ \vdots \\ F^{(n)} \end{bmatrix} \qquad g \triangleq \begin{bmatrix} g^{(1)} \\ \vdots \\ g^{(n)} \end{bmatrix}$$

The equation of motion for one single component S is:

$$M^{(s)}\ddot{u}^{(s)} + K^{(s)}u^{(s)} = F^{(s)} + g^{(s)} \tag{2.2}$$

In Eq. (2.2) M is the symmetric, positive definite mass matrix and K is the symmetric non negative definite stiffness matrix. It states that the sum of the inertia and elastic forces equals the sum of the applied forces and the reaction forces due to the adjacent structure. Dividing the physical coordinates into internal and boundary (coupling) DoF's and assuming that no internal forces are applied, Eq. (2.2) can be partitioned as:

$$\begin{bmatrix} M_{ii}^{(s)} & M_{ic}^{(s)} \\ M_{ci}^{(s)} & M_{cc}^{(s)} \end{bmatrix} \begin{bmatrix} \ddot{u}_i^{(s)} \\ \ddot{u}_c^{(s)} \end{bmatrix} + \begin{bmatrix} K_{ii}^{(s)} & K_{ic}^{(s)} \\ K_{ci}^{(s)} & K_{cc}^{(s)} \end{bmatrix} \begin{bmatrix} u_i^{(s)} \\ u_c^{(s)} \end{bmatrix} = \begin{bmatrix} 0 \\ f_c^{(s)} + g^{(s)} \end{bmatrix} \tag{2.3}$$

At the boundary the forces due to adjacent components should be equilibrated (equilibrium condition) and the displacements are supposed to be equal (compatibility):

$$\begin{aligned} L^T g &= 0 \\ Bu &= 0 \end{aligned} \tag{2.4}$$

[1] The physical models are sometime called the spatial models.

Where,

$$u = Lq = BLq = 0 \tag{2.5}$$

Here $\boldsymbol{q}$ is a unique set of interface and selected internal DoF's and $\boldsymbol{L}$ is the null space of $\boldsymbol{B}$. For the use in the FBS, $\boldsymbol{B}$ is a signed Boolean matrix while $\boldsymbol{L}$ is just a Boolean localization matrix. If the compatibility is satisfied prior to equilibrium the equation of motion for the coupled system yields:

$$\begin{aligned} ML\ddot{q} + Kq &= f + g \\ L^T g &= 0 \end{aligned} \tag{2.6}$$

and premultiplying with $\boldsymbol{L^T}$ gives:

$$\tilde{M}\ddot{q} + \tilde{K}q = \tilde{F} \tag{2.7}$$

where,

$$\tilde{M} = L^T ML \qquad , \tilde{K} = L^T KL \qquad , \tilde{F} = L^T F$$

In dual formulation where the equilibrium is first satisfied the interface forces are defined in the following form:

$$g = -B^T \lambda \tag{2.8}$$

where $\boldsymbol{\lambda}$ corresponds to the interface forces intensities. Due to the construction of the Boolean matrix $\boldsymbol{B}$ the interface forces are equal and in the apposite direction for any pair of coupling (boundary) DoF's:

$$L^T g = -L^T B^T \lambda = 0 \tag{2.9}$$

Substituting Eq. (2.8) in Eq. (2.1) and applying the compatibility, the equation of motion for the dual coupled system becomes:[1]

$$\begin{bmatrix} M & 0 \\ 0 & 0 \end{bmatrix} \begin{bmatrix} \ddot{u} \\ \lambda \end{bmatrix} + \begin{bmatrix} K & B^T \\ B & 0 \end{bmatrix} \begin{bmatrix} u \\ \lambda \end{bmatrix} = \begin{bmatrix} F \\ 0 \end{bmatrix} \tag{2.10}$$

Eq. (2.1)and (2.4) can be transformed into frequency domain using Fourier Transformation and one obtain:

$$Z(\omega)u(\omega) = f(\omega) + g(\omega) \tag{2.11}$$

[1] For detailed derivation see D. de Klerk et al. [2] or D. de Klerk [3].

$$\begin{aligned} Bu(\omega) &= 0 \\ L^T g(\omega) &= 0 \end{aligned} \tag{2.12}$$

$\boldsymbol{Z}$ is known as dynamic stiffness matrix, and in the absence of damping is defined as:

$$Z^{(s)}(\omega) \triangleq -\omega^2 M^{(s)} + K^{(s)} \tag{2.13}$$

Primal assembly of Eq. (2.11) gives:

$$\tilde{Z}q = \tilde{f} \tag{2.14}$$

where:

$$\tilde{Z} = L^T Z L, \qquad \tilde{f} = L^T f \tag{2.15}$$

$$Z = \begin{bmatrix} Z^1 & \cdots & 0 \\ \vdots & \ddots & \vdots \\ 0 & \cdots & Z^n \end{bmatrix} = \begin{bmatrix} (Y^1)^{-1} & \cdots & 0 \\ \vdots & \ddots & \vdots \\ 0 & \cdots & (Y^n)^{-1} \end{bmatrix} \tag{2.16}$$

$\boldsymbol{Y}$ is the dynamic flexibility matrix which equals the inverse of the dynamic stiffness. Primal assembly which is also called Impedance coupling is simply just a summation over the dynamic stiffness's at the boundaries, like in the FEM assembly where the coupling coordinates are added.

Example

For two substructures $\boldsymbol{A}$ and $\boldsymbol{B}$, each having one internal and one coupling coordinates, the primal FBS coupling produce:

$$Z_{total} = L^T \begin{bmatrix} \begin{bmatrix} Y_{ii}{}^A & Y_{ic}{}^A \\ Y_{ci}{}^A & Y_{cc}{}^A \end{bmatrix}^{-1} & 0 \\ 0 & \begin{bmatrix} Y_{cc}{}^B & Y_{ci}{}^B \\ Y_{ic}{}^B & Y_{ii}{}^B \end{bmatrix}^{-1} \end{bmatrix} L = \begin{bmatrix} Z_{ii}{}^A & Z_{ic}{}^A & 0 \\ Z_{ci}{}^A & Z_{cc}{}^A + Z_{cc}{}^B & Z_{ci}{}^B \\ 0 & Z_{ic}{}^B & Z_{ii}{}^B \end{bmatrix} \tag{2.17}$$

where

$$B = [0 \quad 1 \quad -1 \quad 0], \qquad L = \begin{bmatrix} 1 & 0 & 0 \\ 0 & 1 & 0 \\ 0 & 1 & 0 \\ 0 & 0 & 1 \end{bmatrix}$$

2.2 Lagrange Multiplier FBS

With the Lagrange multipliers as the unknown interface forces a given system can be assembled in a dual manner and the assembled system get the following form:

$$\begin{bmatrix} Z & B^T \\ B & 0 \end{bmatrix} \begin{bmatrix} U \\ \lambda \end{bmatrix} = \begin{bmatrix} F \\ 0 \end{bmatrix} \tag{2.18}$$

Solving Eq. (2.18) one obtains:

$$U = Y\left(F - B^T\lambda\right) \tag{2.19}$$

and multiplying with $\boldsymbol{B}$ gives

$$BU = BY\left(F - B^T\lambda\right) = 0 \Leftrightarrow BYB^T\lambda = BYF \tag{2.20}$$

Using Eq. (2.20) an expression for the LM can be obtained which is:

$$\lambda = \left(BYB^T\right)^{-1} BYF \tag{2.21}$$

and substituting Eq. (2.21) into Eq. (2.19) gives:

$$U = Y\left(I - B^T\left(BYB^T\right)^{-1} BY\right)F \tag{2.22}$$

or:

$$\begin{aligned} U &= YF - YB^T\lambda \\ \lambda &= \left(BYB^T\right)^{-1} U_{gap} \\ U_{gap} &= BYF \end{aligned} \tag{2.23}$$

Eq. (2.22) is the formulation of LM FBS and can be interpreted as follows; because of an applied force $\boldsymbol{F}$ a gap $\boldsymbol{U_{gap}}$ is formed between the substructures but the interface forces of intensities $\boldsymbol{\lambda}$ are computed to close this gap. Additional responses associated to the interface forces are specified by $-\boldsymbol{YB^T\lambda}$. The assembled model of the system is:

$$Y_{total} = Y\left(I - B^T\left(BYB^T\right)^{-1} BY\right) \tag{2.24}$$

2.3 Decoupling using LM FBS

Many times an uncoupled substructure should be measured in an assembly. This happens when a substructure cannot be measured separately because it is preloaded or is delicate and needed a fixture. Besides sometimes it is desirable to measure an uncoupled substructure as if, it is in operational condition. The boundary conditions are then made similar to the characteristics of adjacent components by adding masses or springs to the interface for instance.[1] It works (exercise) the substructure locally and gives a better representation of reality.[2]

When lumped-masses are attached to the interface Mass additive normal modes are obtained. Due to attached mass the substructure deforms locally near the interface in the lower substructure mode, which is not possible in the usual free-interface configuration. The resulting free-free modes will therefore satisfy the external constraints applied to the component, guaranteeing the mode shape of the modes. Once the response is measured the effects of the added mass at the interface will be removed.

To remove the fixture or added mass from the substructure prior to the coupling process LM FBS can be utilized. Assume that the impedance representation of the assembly $\boldsymbol{AB}$ and the fixture $\boldsymbol{B}$ are given as:

$$\begin{bmatrix} Z_{aa}^{AB} & Z_{ac}^{AB} & Z_{ab}^{AB} \\ Z_{ca}^{AB} & Z_{cc}^{AB} & Z_{cb}^{AB} \\ Z_{ba}^{AB} & Z_{bc}^{AB} & Z_{bb}^{AB} \end{bmatrix} \begin{bmatrix} u_a \\ u_b \\ u_c \end{bmatrix} = \begin{bmatrix} F_a \\ F_b \\ F_c \end{bmatrix} \tag{2.25}$$

$$\begin{bmatrix} Z_{aa}^{A} & Z_{ac}^{A} \\ Z_{ca}^{A} & Z_{cc}^{A} \end{bmatrix} \begin{bmatrix} u_a^A \\ u_c^A \end{bmatrix} = \begin{bmatrix} F_a^A \\ F_c^A \end{bmatrix} \tag{2.26}$$

Here the subscripts $\boldsymbol{a}$, $\boldsymbol{b}$ and $\boldsymbol{c}$ mean internal to $\boldsymbol{A}$, $\boldsymbol{B}$ and coupling, respectively. In reality the assembly $\boldsymbol{AB}$ is also subjected to connection forces from $\boldsymbol{A}$ and substructure $\boldsymbol{B}$ can be decoupled from $\boldsymbol{A}$ when an additional force is applied to $\boldsymbol{AB}$, such that the total force at connection point is zero. As consequence $\boldsymbol{AB}$ doesn't feels $\boldsymbol{A}$ any more and $\boldsymbol{B}$ is decoupled.[3]

[1] Interface loaded normal modes are introduces by Benfield and Hruda [4]. In this method the presence of the adjacent component is taken into account by using loading in mass and stiffness matrices at the coupling DoF's. The inertial and stiffness loading are the condensed mass and stiffness matrices of the adjacent component. For the condensation is the Guyan reduction applied.

[2] Thinking of a wind turbine, the blades will respond as if they are fixed at the interfaces, because the mass of the blades is just a small fraction of turbine mass.

[3] A very clear illustration of this problem is given by Matthew Allen et al. [5] on page 4895.

With the unknown connection forces due to the presence of $\boldsymbol{A}$ in the $\boldsymbol{AB}$ assembly, Eq. (2.25) and (2.26) are changed into:

$$\begin{bmatrix} Z_{aa}^{AB} & Z_{ac}^{AB} & Z_{ab}^{AB} \\ Z_{ca}^{AB} & Z_{cc}^{AB} & Z_{cb}^{AB} \\ Z_{ba}^{AB} & Z_{bc}^{AB} & Z_{bb}^{AB} \end{bmatrix} \begin{bmatrix} u_a \\ u_b \\ u_c \end{bmatrix} = \begin{bmatrix} F_a \\ F_b \\ F_c \end{bmatrix} - \begin{bmatrix} 0 \\ g_c \\ 0 \end{bmatrix}$$
$$\begin{bmatrix} Z_{aa}^{A} & Z_{ac}^{A} \\ Z_{ca}^{A} & Z_{cc}^{A} \end{bmatrix} \begin{bmatrix} u_a^A \\ u_c^A \end{bmatrix} = \begin{bmatrix} F_a^A \\ F_c^A \end{bmatrix} + \begin{bmatrix} 0 \\ g_c^A \end{bmatrix} \tag{2.27}$$

Defining the Boolean matrix as $\boldsymbol{B} = [\boldsymbol{B}^{\boldsymbol{AB}}\ \boldsymbol{B}^{\boldsymbol{A}}] = [\boldsymbol{0}\ \boldsymbol{I}\ \boldsymbol{0}\ \boldsymbol{0}\ \boldsymbol{-I}]$ and choosing the interface forces as $\boldsymbol{g}=\boldsymbol{B}^{\boldsymbol{T}}\boldsymbol{\lambda}$ the dual assembly of $\boldsymbol{AB}$ and $\boldsymbol{A}$ becomes:[1]

$$\begin{bmatrix} Z^{AB} & 0 & B^{AB^T} \\ 0 & -Z^A & B^{A^T} \\ B^{AB} & B^A & 0 \end{bmatrix} \begin{bmatrix} u^{AB} \\ u^A \\ \lambda \end{bmatrix} = \begin{bmatrix} F^{AB} \\ -F^A \\ 0 \end{bmatrix} \tag{2.28}$$

Eq. (2.28) states that the decoupling problem corresponds to the dual assembly of the negative dynamic stiffness of the fixture. Solving $\boldsymbol{\lambda}$ using the compatibility condition and assuming that $\boldsymbol{F^A=0}$, the decoupled response is:[2]

$$u^{AB} = Y^{AB}F^{AB} - Y^{AB}B^{AB^T}Z_{\text{int}}u_{\text{int}} \tag{2.29}$$

where

$$Z_{\text{int}} = \left(B^{AB}Y^{AB}B^{AB^T} - B^AY^AB^{A^T} \right)$$
$$u_{\text{int}} = B^{AB}Y^{AB}F^{AB} \tag{2.30}$$

Eq. (2.29) can be interpreted as follows; $\boldsymbol{Y^{AB}F^{AB}}$ is the response of the assembled system, this lead to interface displacement $\boldsymbol{U_{int}}$. The corrected interface dynamic stiffness matrix $\boldsymbol{Z_{int}}$ eliminates the influences of the fixture at interface and $\boldsymbol{Z_{int}U_{int}}$ leads to correction forces. These forces ensure that the interface displacement is just related to the dynamic stiffness of $\boldsymbol{B}$ and not to that of $\boldsymbol{AB}$ and are spread to other DoF's through multiplication by $\boldsymbol{Y^{AB}(B^{AB})^T}$.

[1] Note! In decoupling it is also possible to impose compatibility constrains on the internal DoF's. It would improve the decoupling when the substructure $\boldsymbol{A}$ has also internal DoF's and will lead to slightly different formulation. See for more details S.N. Voormeeren et al. [6]

[2] For detailed derivation see S.N. Voormeeren et al. [6]

3 Inertia Properties, Rotational DoF's and noise

The measured FRF's contain a considerable amount of information, much more than any other models and they can be directly used to couple the substructures. They have the advantage of including all structural information, damping and the effect of the higher modes. But regardless these advantages, some difficulties are associated with tem. Among those rigid body modes, rotational coordinates, noise and experimental errors can be mentioned.

In the field of DS sometimes just the rigid body dynamics are enough to make a model. The mass, the location of centre of gravity and the moments of inertia are necessary and sufficient information to calculate the mass normalized rigid body modes and with that the rigid body dynamic. In analytical terms these properties can be easily obtained but dealing with substructures for which no analytical models are available they should be defined through experimental routine and appropriate methods. One of these methods is known as Inertia Restraint Method (IRM). It employs the impact measurement data in the frequency domain and is applicable to substructures where the rigid body and flexible modes are well separated.[1] IRM uses the fact that all inertia properties are condensed into the mass line (inertia restraint) of a freely supported structure.

Rotational DoF's are very difficult to excite and neglecting them provides meaningless result, if the coupling is performed through a single point. To cope with this problem the Interface Deformation Modes (IDM) formulation can be applied.[2] It mapped the measured translational coordinates, in least square sense, to an admissible space

[1] See R.A.B. Almaida et al. [7]

[2] See D. de Klerk [3]

spanned by local interface modes in order to attain the RDoF's. It returns a virtual point including the RDoF's which can serve as coupling point.

The experimental errors are principally the measurement errors which are associated with; sensor positioning and alignment, signal processing errors, like leakage and bias errors due to limited frequency resolution, added mass introduced by measurement equipment, Local properties of the structure like damping in the joints and damping and stiffness of the suspension.

In this chapter it is shown how inertia properties of a body can be determined from impact measurement and how the accuracy of the results can be improved.

Then is explained and shown how the RDoF's can be obtained by means of IDM and how it can also serve as a filter.

At the end of the chapter troubles associated with the noise and inconsistency are highlighted and is recommended how to minimize inconsistency.

3.1 Measuring Inertia properties

The equation of motion of a rigid body around an arbitrary point $\underline{o}$ attached to the body is given with:[1]

$$\begin{aligned} m\ddot{r}_o - mr_{og} \times \dot{\omega} &= F - m\omega \times \left(\omega \times r_{og}\right) \\ mr_{og} \times \ddot{r}_o + J_o \cdot \dot{\omega} &= t - \omega \times \left(J_o \cdot \omega\right) \end{aligned} \tag{3.1}$$

where

m = Total mass
$\ddot{r}_o$ = Absolute acceleration in the inertial reference frame
r_{og} = Vector from point $\underline{o}$ to the centre of gravity g
$\dot{\omega}$ = The vector of angular velocities
J_o = Inertia tensor with respect to point $\underline{o}$

F and **t** are the applied external forces and moments. Using the Bryant successive angle rotation transformation Eq. (3.1) can be transformed, from the inertial reference frame (global coordinates) into the body fixed frame (local coordinates). Assuming small rotational velocities and very small angular motion the equation of motion in the fixed body frame becomes:[2]

$$M_r^o \ddot{X}^o = F^o \tag{3.2}$$

where

$$M_r^o = \begin{bmatrix} m & 0 & 0 & 0 & mz_{og} & -my_{og} \\ 0 & m & 0 & -mz_{og} & 0 & mx_{og} \\ 0 & 0 & m & my_{og} & -mx_{og} & 0 \\ 0 & -mz_{og} & my_{og} & J_{xx}{}^o & -J_{xy}{}^o & -J_{xz}{}^o \\ mz_{og} & 0 & -mx_{og} & -J_{yx}{}^o & J_{yy}{}^o & -J_{yz}{}^o \\ -my_{og} & mx_{og} & 0 & -J_{zx}{}^o & -J_{zy}{}^o & J_{zz}{}^o \end{bmatrix} \quad \ddot{X}^o = \begin{bmatrix} \ddot{x}^o \\ \ddot{y}^o \\ \ddot{z}^o \\ \ddot{\theta}_x^o \\ \ddot{\theta}_y^o \\ \ddot{\theta}_z^o \end{bmatrix} \tag{3.3}$$

Knowing the geometrical relation between point $\underline{o}$ and arbitrary point β on the same body, for point β one may write:

$$\ddot{X}_\beta = T_{o\beta} \ddot{X}^o \tag{3.4}$$

[1] See Jens Wittenburg [8] page 40 or Carsten Schedlinski [9]

[2] For the detailed derivation see Carsten Schedlinski [9]

where

$$T_{o\beta}=\begin{bmatrix} I & R_{o\beta} \\ 0 & I \end{bmatrix} \qquad R_{o\beta}=\begin{bmatrix} 0 & z_{o\beta} & -y_{o\beta} \\ -z_{o\beta} & 0 & x_{o\beta} \\ y_{o\beta} & -x_{o\beta} & 0 \end{bmatrix} \tag{3.5}$$

Matrix $\boldsymbol{T}$ is known as geometrical transformation matrix and has the following properties:

$$\begin{aligned} T_{o\beta}{}^{-1} = T_{\beta o} &= \begin{bmatrix} I & R_{\beta o} \\ 0 & I \end{bmatrix} = \begin{bmatrix} I & -R_{o\beta} \\ 0 & I \end{bmatrix} \\ T_{og}{}^{-T} = T_{go}{}^{T} &= \begin{bmatrix} I & 0 \\ R_{o\beta} & I \end{bmatrix} \end{aligned} \tag{3.6}$$

Theoretically when at least six TDoF's, at three separated nodes on a body, which are not lying on a line, are known the acceleration vector at any given point can be determined. In experimental terms, having measured three translations at $\boldsymbol{n}$ points, for one single excitation $\boldsymbol{f}$, one may write:

$$\begin{bmatrix} \begin{Bmatrix} \ddot{x}_1 \\ \ddot{y}_1 \\ \ddot{z}_1 \end{Bmatrix} \\ \vdots \\ \begin{Bmatrix} \ddot{x}_n \\ \ddot{y}_n \\ \ddot{z}_n \end{Bmatrix} \end{bmatrix}_f = \begin{bmatrix} \begin{bmatrix} 1 & 0 & 0 & 0 & z_{o1} & -y_{o1} \\ 0 & 1 & 0 & -z_{o1} & 0 & x_{o1} \\ 0 & 0 & 1 & y_{o1} & -x_{o1} & 0 \end{bmatrix} \\ \vdots \\ \begin{bmatrix} 1 & 0 & 0 & 0 & z_{on} & -y_{on} \\ 0 & 1 & 0 & -z_{on} & 0 & x_{on} \\ 0 & 0 & 1 & y_{on} & -x_{on} & 0 \end{bmatrix} \end{bmatrix} \begin{bmatrix} \ddot{x}^o \\ \ddot{y}^o \\ \ddot{z}^o \\ \ddot{\theta}^o_x \\ \ddot{\theta}^o_y \\ \ddot{\theta}^o_z \end{bmatrix}_f \tag{3.7}$$

$$\begin{bmatrix} \ddot{x}^o \\ \ddot{y}^o \\ \ddot{z}^o \\ \ddot{\theta}^o_x \\ \ddot{\theta}^o_y \\ \ddot{\theta}^o_z \end{bmatrix}_f = \left(\begin{bmatrix} I & R_{o1} \\ \vdots & \\ I & R_{on} \end{bmatrix}^T \begin{bmatrix} I & R_{o1} \\ \vdots & \\ I & R_{on} \end{bmatrix} \right)^{-1} \begin{bmatrix} I & R_{o1} \\ \vdots & \\ I & R_{on} \end{bmatrix}^T \begin{bmatrix} \begin{Bmatrix} \ddot{x}_1 \\ \ddot{y}_1 \\ \ddot{z}_1 \end{Bmatrix} \\ \vdots \\ \begin{Bmatrix} \ddot{x}_n \\ \ddot{y}_n \\ \ddot{z}_n \end{Bmatrix} \end{bmatrix}_f \tag{3.8}$$

Eq. (3.8) computes the acceleration vector at point $\underline{o}$ in a least square sense for one excitation and can be used to solve Eq. (3.2). Eq. (3.2) can be rewritten as: [1]

[1] See Antonio P.V. Urgiera [10]

$$\left[\begin{array}{cccc|cccccc} \ddot{x}^o & 0 & -\ddot{\theta}_z^o & \ddot{\theta}_y^o & 0 & 0 & 0 & 0 & 0 & 0 \\ \ddot{y}^o & \ddot{\theta}_z^o & 0 & -\ddot{\theta}_x^o & 0 & 0 & 0 & 0 & 0 & 0 \\ \ddot{z}^{\ddot{o}} & -\ddot{\theta}_y^o & \ddot{\theta}_x^o & 0 & 0 & 0 & 0 & 0 & 0 & 0 \\ \hline 0 & 0 & \ddot{z}^o & -\ddot{y}^o & \ddot{\theta}_x^o & -\ddot{\theta}_y^o & -\ddot{\theta}_z^o & 0 & 0 & 0 \\ 0 & -\ddot{z}^o & 0 & \ddot{x}^o & 0 & -\ddot{\theta}_x^o & 0 & \ddot{\theta}_y^o & -\ddot{\theta}_z^o & 0 \\ 0 & \ddot{y}^o & -\ddot{x}^o & 0 & 0 & 0 & -\ddot{\theta}_x^o & 0 & -\ddot{\theta}_y^o & \ddot{\theta}_z^o \end{array}\right]_f \left[\begin{array}{c} m \\ x'_{og} \\ y'_{og} \\ z'_{og} \\ J_{xx}{}^o \\ J_{xy}{}^o \\ J_{xz}{}^o \\ J_{yy}{}^o \\ J_{yz}{}^o \\ J_{zz}{}^o \end{array}\right] = \left[\begin{array}{c} F_x \\ F_y \\ F_z \\ t_x^o \\ t_y^o \\ t_z^o \end{array}\right]_f \tag{3.9}$$

where

$$\left[\begin{array}{c} F_x \\ F_y \\ F_z \\ t_x^o \\ t_y^o \\ t_z^o \end{array}\right]_f = \left[\begin{array}{c} I \\ R_{of}^T \end{array}\right] \left[\begin{array}{c} F_x \\ F_y \\ F_z \end{array}\right]_f, \qquad \begin{array}{l} x'_{og} = mx_{og} \\ y'_{og} = my'_{og} \\ z'_{og} = mz'_{og} \end{array} \tag{3.10}$$

After substituting the outcomes of Eq. (3.8) into Eq. (3.9) all ten inertia properties can be determined directly. In theory Eq. (3.9) can be solved if a set of minimum two independent excitations have been carried out. When all ten unknowns are calculated the inertia tensor at the centre of gravity can be calculated with:

$$J^g = J^o - R_{og} m R_{go} \tag{3.11}$$

The principal axis can be obtained from $\boldsymbol{J}^g$ by solving an eigenvalue problem. Improved accuracy can be achieved when the mass and the centre of mass are known in advance. These values can be obtained with static tests. Also the measurement and excitation point selection should be taken in consideration. For instance having three measurement points, better results might be obtained if they form a regular triangle.[1]

The excitation points are recommended to have a certain condition such that; their directions are mutually orthogonal, their extension lines do not intersect, their extension lines are located as far as possible from the centre of gravity.

[1] See Hyuk Lee et al. [11]

3.2 Rotational DoF's

To tackle and cope with the RDoF's issue IDM can be used. When the interface is assumed to be rigid, a minimum of six translational DoF's at three nodes are sufficient to describe the motion of a rigid interface locally and with that of a coupling node on that interface. The equation of motion of a substructure in the frequency domain is:

$$U = YF \tag{3.12}$$

Partitioning Eq. (3.12) into internal and coupling (boundary) DoF's gives:

$$\begin{bmatrix} u_i \\ u_c \end{bmatrix} = \begin{bmatrix} Y_{ii} & Y_{ic} \\ Y_{ci} & Y_{cc} \end{bmatrix} \begin{bmatrix} F_i \\ F_c \end{bmatrix} \tag{3.13}$$

With the Matrix $\boldsymbol{R}$, which contains a selected set of interface deformations modes Eq. (3.13) can be written as:

$$\begin{bmatrix} u_i \\ u_c \end{bmatrix} = \begin{bmatrix} I & 0 \\ 0 & R \end{bmatrix} \begin{bmatrix} u_i \\ q \end{bmatrix} + \begin{bmatrix} 0 \\ r \end{bmatrix} \tag{3.14}$$

$$\begin{bmatrix} f_i \\ f_c \end{bmatrix} = \begin{bmatrix} I & 0 \\ 0 & R \end{bmatrix} \begin{bmatrix} f_i \\ m \end{bmatrix} + \begin{bmatrix} 0 \\ r_f \end{bmatrix} \tag{3.15}$$

$\boldsymbol{m}$ is the resultant forces and moments relative to the point around which the rigid modes are defined. The residual motion and residual forces $\boldsymbol{r}$ and $\boldsymbol{r_f}$, due to the truncation of the deformation mode set, are orthogonal to the space spanned by $\boldsymbol{R}$. Making use of orthogonality properties one may write:

$$u = G\tilde{u} + \begin{bmatrix} 0 \\ r \end{bmatrix} \Rightarrow \tilde{u} = \left(G^T G\right)^{-1} G^T u \tag{3.16}$$

$$f = G\tilde{f} + \begin{bmatrix} 0 \\ r_f \end{bmatrix} \Rightarrow \tilde{f} = \left(G^T G\right)^{-1} G^T f \tag{3.17}$$

where

$$G = \begin{bmatrix} I & 0 \\ 0 & R \end{bmatrix} \qquad \tilde{u} = \begin{bmatrix} u_i \\ q \end{bmatrix} \qquad \tilde{f} = \begin{bmatrix} f_i \\ m \end{bmatrix} \tag{3.18}$$

Substituting Eq. (3.16) in Eq. (3.13) and using Eq. (3.17) gives the expression of the reduced space of motion:

$$\tilde{u} = TYT^T f_r = \tilde{Y} f_r \tag{3.19}$$

where

$$\begin{aligned} T &= \left(G^T G\right)^{-1} G^T \\ \tilde{Y} &= TYT^T \\ f_r &= G^T f \end{aligned} \tag{3.20}$$

Usually each set of boundary coordinates $\boldsymbol{u_b}$ consist of three nodes which encircle the virtual point $\boldsymbol{q}$. The location of these points relative to each other could influence the end result as the reduction basis $\boldsymbol{R}$ is defined from geometrical relations. In the case where just rigid body modes are considered in the reduction basis, for three nodes with nine TDoF's, $\boldsymbol{R}$ is:

$$\begin{bmatrix} u_{1x} \\ u_{1y} \\ u_{1z} \\ u_{2x} \\ u_{2y} \\ u_{2z} \\ u_{3x} \\ u_{3y} \\ u_{3z} \end{bmatrix} = \begin{bmatrix} 1 & 0 & 0 & 0 & r_{1z} & -r_{1y} \\ 0 & 1 & 0 & -r_{1z} & 0 & r_{1x} \\ 0 & 0 & 1 & r_{1y} & -r_{1x} & 0 \\ 1 & 0 & 0 & 0 & r_{2z} & -r_{2y} \\ 0 & 1 & 0 & -r_{2z} & 0 & r_{2x} \\ 0 & 0 & 1 & r_{2y} & -r_{2x} & 0 \\ 1 & 0 & 0 & 0 & r_{3z} & -r_{3y} \\ 0 & 1 & 0 & -r_{3z} & 0 & r_{3x} \\ 0 & 0 & 1 & r_{3y} & -r_{3x} & 0 \end{bmatrix} \begin{bmatrix} q_x \\ q_y \\ q_z \\ q_{\theta_x} \\ q_{\theta_y} \\ q_{\theta_z} \end{bmatrix} + \mathbf{r} \tag{3.21}$$

This basis will reduce and map the selected coordinates to a virtual point in a least square sense. In the matrix notation Eq. (3.19) is written as:

$$\begin{bmatrix} u_i \\ q \end{bmatrix} = \begin{bmatrix} Y_{ii} & Y_{ic} R \left(R^T R\right)^{-1} \\ \left(R^T R\right)^{-1} R^T Y_{ci} & \left(R^T R\right)^{-1} R^T Y_{cc} R \left(R^T R\right)^{-1} \end{bmatrix} \begin{bmatrix} f_i \\ m \end{bmatrix} \tag{3.22}$$

The original set of coordinates is retrieved with:

$$\begin{bmatrix} u_i \\ u_c \end{bmatrix} = \begin{bmatrix} Y_{ii} & Y_{ic} R \left(R^T R\right)^{-1} R^T \\ R \left(R^T R\right)^{-1} R^T Y_{ci} & R \left(R^T R\right)^{-1} R^T Y_{cc} R \left(R^T R\right)^{-1} R^T \end{bmatrix} \begin{bmatrix} f_i \\ f_c \end{bmatrix} \tag{3.23}$$

If the interface is really rigid, applying Eq. (3.22) and Eq. (3.23) successively to a data set, will remove the noise and IDM works as a filter; it maps the data set to a space in a least square sense and rotate it back to its original space and hence noise is removed.

3.3 Preparing and monitoring the measurement

The coupling and decoupling formulations are very sensitive to experimental errors. Condition numbers of the measured FRF's are very high around the resonance frequency which makes the matrix inversion very sensitive to the uncertainties and measurement noise and amplifies them to the coupled system. Decoupling is in particular sensitive around the anti-resonances of the known subsystems, while coupling is most sensitive around the resonance frequencies of the subsystems.[1]

The errors and inaccuracies are incorporated in the measured data set because of cross-axis sensitivity of sensors, inaccuracies in measurement chain, mass loading and misalignment of the sensors and can be divided in two groups; inconsistencies and random measurement noise.

The inconsistencies are mainly caused by varying additional mass and stiffness effects, which result in incoherent modal content and slightly different entities of the response model[2]. These effects will cause spurious peaks in the assembled structure in the vicinity of substructure eigenfrequency or will modify the resonances and anti-resonances in the assembled configuration.[3]

To avoid inconsistencies when the hammer is roved, care should be given to anti resonances. Anti-resonances are local parameters and they vary for each pair of excitation and response and are sensitive to the exact location of excitation. When the sensor is roved, measurement points except for the actual measurement point should be supplied with dummy masses to avoid reciprocity problem.[4]

Having a good measurement set up during the measurement, the coherence and the driving point response should be monitored. The coherence function provides a measure of linearity between the input and output. For values less than one, one may think of; additional external signal source or additional input, measurement noise, leakage not reduced by windowing, system non linearity, noise on output and shifted anti resonances.

The most informative part of the measured response is its imaginary part. It shows both the amplitude and direction of the response. The excitation and response direction are same for a driving point thus the imaginary part of driving point should always be positive for accelerance measurement.

---

[1] See S.N. Voormeeren et al. [12]

[2] Such as discrepancy in the resonance frequencies, damping factors and shifting of the mode shapes.

[3] See Daniel. J. Rixen [13]

[4] The FRF Matrix is symmetric and this will be recognized as principle of reciprocity.

4 Cyclic Symmetric Structure

Many structures exhibit translational or rotational periodicity and can be thought of as being composed of identical substructures. Typical structures with rotational periodicity are; turbine disk, vehicle wheels or wind turbines. They are usually named Cyclic Symmetric structures (CSS) and if their symmetry property is properly used they can be measured or computed extremely efficient.

In analytical terms these structures are first cut into identical pieces with their own local coordinates. Just one piece is modeled and computed. The results are then post processed to attain the dynamic of the whole structure.

In experimental terms the structure is divided virtually into several identical sections with their own local coordinates. Taking full advantage of the symmetric properties like axisymmetry, a minimum number of coordinates are then measured and used to build up and synthesize a full model.

In this chapter the key aspects behind the CSS synthesizing from a minimum number of measured coordinates are illustrated.

First the notion of coordinate transformations in the measurement field is treated. Then a method is proposed which defines the full substructure model from a minimum number of measured local coordinates and thereafter it is explained how to synthesize a lumped model based on inertia properties when dealing with CSS.

All the techniques are illustrated and described as they have been derived to be applied to a wind turbine hub but they can be generalized and be used for any kind of CSS.

4.1 Coordinates transformation

The measurement and excitation directions are not always predefined. For instance when curved structures like wind turbine blades are to be measured each measurement point has its own local coordinates. Also sometimes it is a need to measure a structure at several spots in different local coordinates when the symmetry properties are going to be utilized. Figure 4-1 shows such a situation where the arrows indicate the direction of measurement or/and excitation.

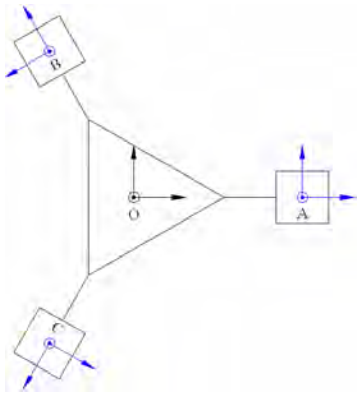

Figure 4-1; A structure being measured in different local coordinates

For identification purposes, Operational Deflection Shape (ODS) or mode shape visualization the obtained FRF's should then be transformed into global direction. The equations of motion in the global and local directions are given respectively with:

$$u_g = Y_g F_g \tag{4.1}$$

$$u_l = Y_l F_l \tag{4.2}$$

The relation between the local and global response and local and global excitation is:

$$u_l = R_u u_g \Leftrightarrow u_g = R_u^{-1} u_l \tag{4.3}$$

$$F_l = R_f F_g \tag{4.4}$$

Substituting Eq. (4.3) in (4.1) and Eq. (4.2) in (4.4) yield:

$$Y_g F_g = R_u^{-1} u_l \tag{4.5}$$

$$u_l = Y_l R_f F_g \tag{4.6}$$

Eq. (4.5) together with (4.6) give:

$$Y_g F_g = R_u^{-1} Y_l R_f F_g \tag{4.7}$$

$\boldsymbol{R_u}$ and $\boldsymbol{R_f}$ are rotation matrixes so it holds that $\boldsymbol{R_u^{-1}=R_u^T}$. The measured local FRF's can be transformed into global direction using Eq. (4.7) and the transformed FRF in the global direction becomes:

$$Y_g = R_u^T Y_l R_f \tag{4.8}$$

4.2 CSS Synthesizing

The periodic structures which are cyclic symmetric like airplane propeller, bladed disk or wind turbines are axisymmetric and exhibit structural properties and geometry which are rotationally periodic. To understand the nature of this kind of structure lets first look into the circulant matrices. A matrix is said to be circulant if their columns are obtained from one vector and its cyclic permutations:

$$C = circ[c_1, c_2, ..., c_n] = \begin{bmatrix} c_1 & c_n & \cdots & c_3 & c_2 \\ c_2 & c_1 & \cdots & c_4 & c_3 \\ \vdots & \vdots & \ddots & \vdots & \vdots \\ c_{n-1} & c_{n-2} & \cdots & c_1 & c_n \\ c_n & c_{n-1} & \cdots & c_2 & c_1 \end{bmatrix} \tag{4.9}$$

$\boldsymbol{C}$ has $\boldsymbol{n}$ distinct elements. When $\boldsymbol{C}$ is symmetric and circulant, the number of distinct elements is $\boldsymbol{(n+2)/2}$, when $\boldsymbol{n}$ is even and $\boldsymbol{(n+1)/2}$, when $\boldsymbol{n}$ is odd.

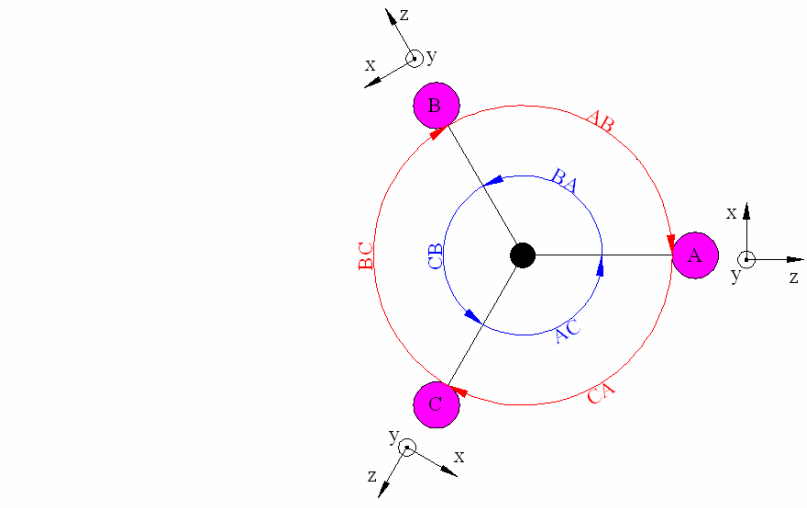

Figure 4-2; Schematic representation of a Cyclic Symmetric Structure

Imagine a structure as it is shown in Figure 4-2, which consists of three identical sectors, ***A***, ***B*** and ***C***. The dynamic flexibility of the full structure is:

$$Y_{tot} = \begin{bmatrix} Y_{AA} & Y_{AB} & Y_{AC} \\ Y_{BA} & Y_{BB} & Y_{BC} \\ Y_{CA} & Y_{CB} & Y_{CC} \end{bmatrix} \tag{4.10}$$

Using the properties of the cyclic structure and utilizing the facts that when the structure has been measured in the local direction $\boldsymbol{Y_{AB}=Y_{CA}=Y_{BC}}$ and $\boldsymbol{Y_{BA}=Y_{CB}=Y_{AC}}$, as indicated by the bowed arrows in Figure 4-2, Eq. (4.10) becomes:

$$Y_{ABC} = \begin{bmatrix} Y_{AA} & Y_{AB} & Y_{BA} \\ Y_{BA} & Y_{AA} & Y_{AB} \\ Y_{AB} & Y_{BA} & Y_{AA} \end{bmatrix} \tag{4.11}$$

According to Eq. (4.11) the Inertance (Receptance, Mobility or Accelerance) matrix is circulant and just by measuring one driving point and one cross FRF the full model of a CSS can be constructed. This may shorten the measurement time and ensures the reciprocity of the full model.

4.3 Inertia properties and Lumped CSS model

Imagine a cyclic symmetric system as shown in Figure 4-3. It represents schematically a hub with three junctions ***A***, ***B*** and ***C***. The global coordinate system is named ***hub*** and is located at the geometric center of the hub. One of its axes is aligned with the hub rotational axis which is automatically a principal axis.

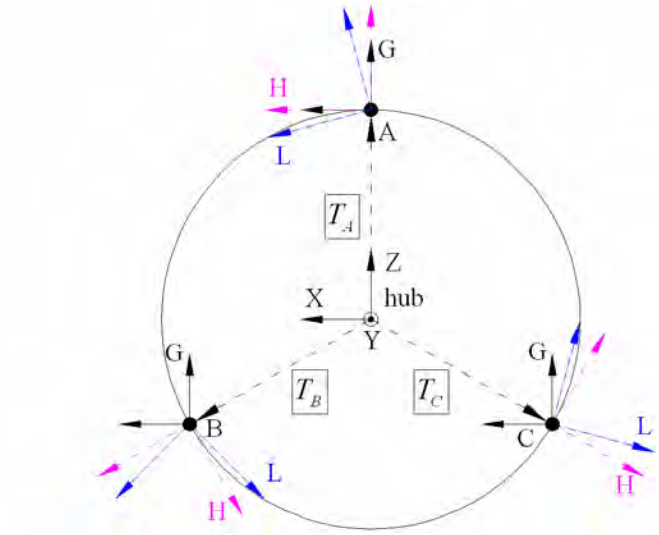

Figure 4-3; Defined coordinates system in the hub

At the hub joints three other coordinate systems are defined. The first one is called $\boldsymbol{G}$ and is aligned with the global coordinate. The second coordinate system is an intermediate coordinate system between the $\boldsymbol{G}$ and the local coordinate system of each joint and is indicated with $\boldsymbol{H}$. The third and the last coordinate system is the local coordinate system and is labeled with $\boldsymbol{L}$.

When the hub is modeled as a point mass with six DoF's along the rotational axis and the full receptance of the hub is required at the hub joints, the response model of the point mass at that given point should be expanded to the joints. Because of periodicity and symmetry of the hub just two matrix elements are sufficient and necessary to build up the full receptance matrix as told in section 4.2. For instance let take $\boldsymbol{Y_{AA}}$ and $\boldsymbol{Y_{AB}}$.

In order to calculate $\boldsymbol{Y_{AA}}$, first the applied forces at point $\boldsymbol{A}$ should be transformed and transported to the ***hub***, where after the acceleration can be computed. Once this is done using the geometrical relations the computed accelerations at ***hub*** can be transported and transformed back to $\boldsymbol{A}$ and $\boldsymbol{Y_{AA}}$ can be synthesized. The transformation of the applied forces from the local coordinated at $\boldsymbol{A}$ to global forces at ***hub*** is given with:[1]

$$\begin{aligned} F_A^H &= R_A^{HL^T} F_A^L \\ F_A^G &= R_A^{GH^T} F_A^H = R_A^{GH^T} R_A^{HL^T} F_A^L \\ F_A^{hub} &= T_A^T F_A^G = T_A^T R_A^{GH^T} R_A^{HL^T} F_A^L \end{aligned} \tag{4.12}$$

The accelerations due to these forces at the hub center, which is assumed rigid, are:

$$\alpha_A^{hub} = M^{-1} F_A^{hub} \tag{4.13}$$

Using Eq. (4.13) the acceleration at the local coordinates can be computed with:

$$\begin{aligned} \alpha_A^G &= T_A \alpha_A^{hub} \\ \alpha_A^H &= R_A^{GH} \alpha_A^G = R_A^{GH} T_A \alpha_A^{hub} \\ \alpha_A^L &= R_A^{HL} \alpha_A^H = R_A^{HL} R_A^{GH} T_A \alpha_A^{hub} \end{aligned} \tag{4.14}$$

Substituting Eq. (4.13) and (4.12) into (1.2) gives:

$$\alpha_A^L = R_A^{HL} R_A^{GH} T_A M^{-1} T_A^T R_A^{GH^T} R_A^{HL^T} F_A^L \tag{4.15}$$

and finally the block matrix $\boldsymbol{Y_{AA}}$ can be computed with:

$$Y_{AA} = R_A^{HL} R_A^{GH} T_A M^{-1} T_A^T R_A^{GH^T} R_A^{HL^T} \tag{4.16}$$

[1] D.J Rixen, Private Notes, March, 2012.

The hub is an axisymmetric structure and is invariant to any rotation around the rotational axis (cylindrical axis):

$$R_B^{GH\,T} M^{-1} R_B^{GH} = R_C^{GH\,T} M^{-1} R_C^{GH} = M^{-1} \tag{4.17}$$

Now imagine the hub being rotated clockwise $-2\pi/3$ as shown in Figure 4-4. It emphasis that $\boldsymbol{B}$ is becoming $\boldsymbol{A}$, $\boldsymbol{A}$ is becoming $\boldsymbol{C}$ and that $\boldsymbol{Y_{AB}}$ is the same as $\boldsymbol{Y_{CA}}$.

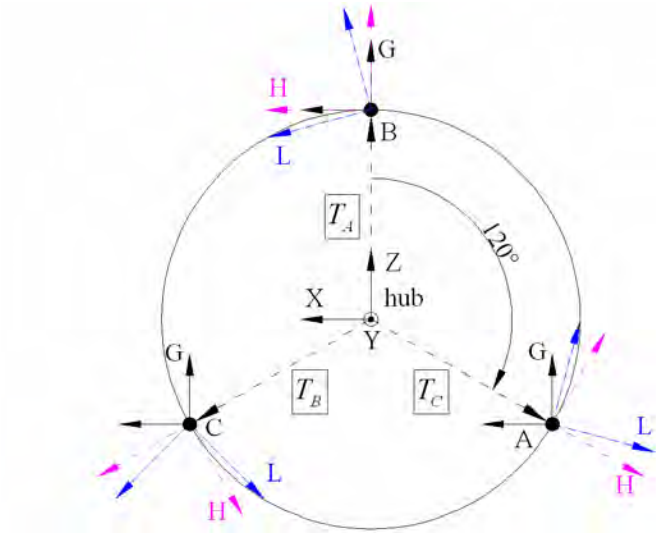

Figure 4-4; Hub being rotated -120°

Using the same procedure as given in Eq. (4.12) through Eq. (4.15) one may write:

$$Y_{AB} = R_C^{HL} R_C^{GH} T_C M^{-1} T_A^T R_A^{GH\,T} R_A^{HL\,T} \tag{4.18}$$

$\boldsymbol{T_A}$, $\boldsymbol{T_B}$ and $\boldsymbol{T_C}$ are matrices which are built on the vectors from point ***hub*** to points $\boldsymbol{A}$, $\boldsymbol{B}$ and $\boldsymbol{C}$, respectively and are also known as geometrical transformation matrix and:

$$\begin{aligned} T_B &= R_B^{GH\,T} T_A R_B^{GH} \\ T_C &= R_C^{GH\,T} T_A R_C^{GH} \end{aligned} \tag{4.19}$$

After substituting Eq. (4.19) into (4.18) the formulation of the block matrix $\boldsymbol{Y_{AB}}$ becomes:

$$Y_{AB} = R_C^{HL} T_A R_C^{GH} M^{-1} T_A^T R_A^{GH\,T} R_A^{HL\,T} \tag{4.20}$$

Having the inertia properties, using Eq. (4.11) with (4.16) and (4.20) the lumped CSS model with three joint can be synthesized. For the definition of $\boldsymbol{M}$ see Eq. (3.3). $\boldsymbol{M^{-1}}$ is the dynamic flexibility of a rigid body.

5 Experimental DS Test bed

To predict the structural dynamic of a system several DS techniques are developed in the course of time. They allow local optimization and monitor the local and global dynamic which can prevent structural damage and increase the lifetime.

The models used in those techniques are or analytically or experimentally derived. The experimentally derived models are sometimes cheaper and faster to obtain and they may represent the actual substructures better. Perceiving these facts, in order to advance the experimental DS technology and theory and compare the existing methods Ampair 600 wind turbine is candidate by the SEM substructuring focus group like a test bed.

Figure 5-1; Ampair wind turbine

The Ampair 600 wind turbine consists of three blades, hub, nacelle, tower and the base. See Figure 5-1. The total mass is ***114 [kg]***.[1] It is ***1.85 [m]*** high is supported on a trampoline freely. The nacelle itself consists of the housing, mock generator, front bearing retainer and the tail fin. Some modifications are made to certain substructures to let them behave more linearly. The pitch mechanism is fixed and the generator is parked and don't rotate.

Delft University of Technology has decided to initiate the first iteration by substructuring the hub and three blades. The full wind turbine model will be available after several iterations. Therefore the substructures model and the assembly results presented in this work are the results of the first iteration. It outlines and describes the measurement process and each intermediate step towards the blade and hub model and the assembly results.[2] The final assembly is shown in Figure 5-2.

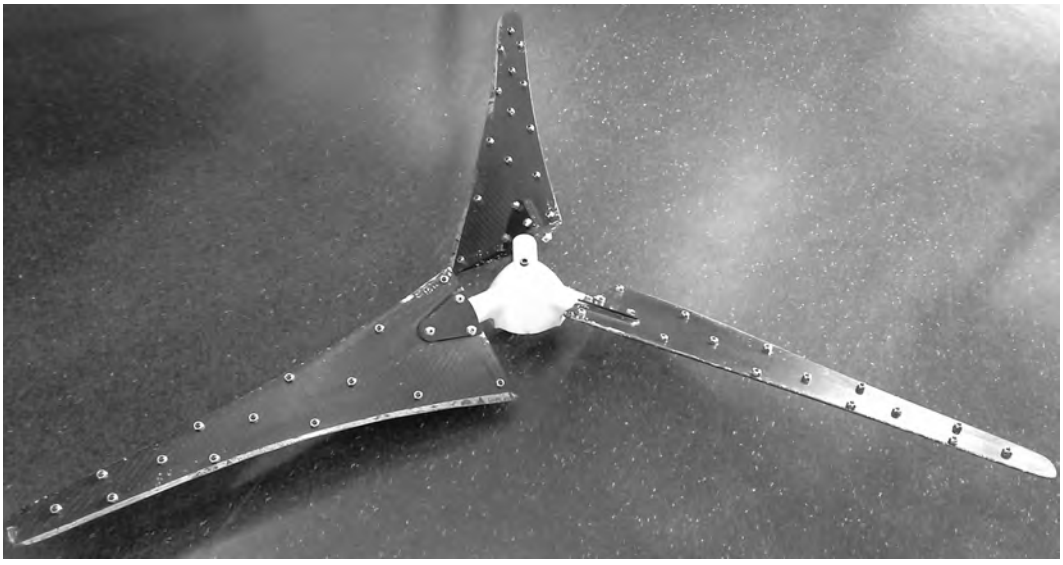

Figure 5-2; Hub-Blades assembly

In this chapter the physical and geometrical properties of the substructures are briefly summarized. The local and the global coordinate systems are defined and the measurement strategies are given. Besides a very short description of the fixture is given which is used during the blade measurements.

[1] See Randy L. Mayes [14]

[2] All the measurements are done in free configuration with the same sampling rate and frequency resolution of ***0.25 Hz***. The band width is ***1600 Hz*** but the assembly results are discussed and evaluated up to ***185 Hz***.

5.1 The Blades

Blades are glass reinforced polyester structures. They have a complex and curved geometry. The material properties are not homogeneous and the structure is sandwiched. The global coordinates of the blades is shown in Figure 5-3. The blades show almost the same dynamic behavior and therefore just one single blade is modeled and is three times used in the assembly process.[1]

The sensors together with dummy masses are roved to measure the blades. No Roving Hammer is applied because of enormous blade tip flexibility which results easily in double hit and/or bad coherence. Besides, roving the sensors appears to be the only way to hit the blades in all three directions. The measurements are relatively consistent in terms of added mass since dummy masses are used, which have the same mass as the used acceleration sensors. Each of them weights approximately ***6.8 [g]*** which makes each blade ***95 [g]*** heavier. The blade together with the dummy masses weights ***0.9 [kg]***. In total twenty points are measured from which six are located at blade root holes where the bolt going through. The other fourteen points are distributed over the surface of the blade which catches the wind when the wind turbine is in operation. See Figure 5-3.

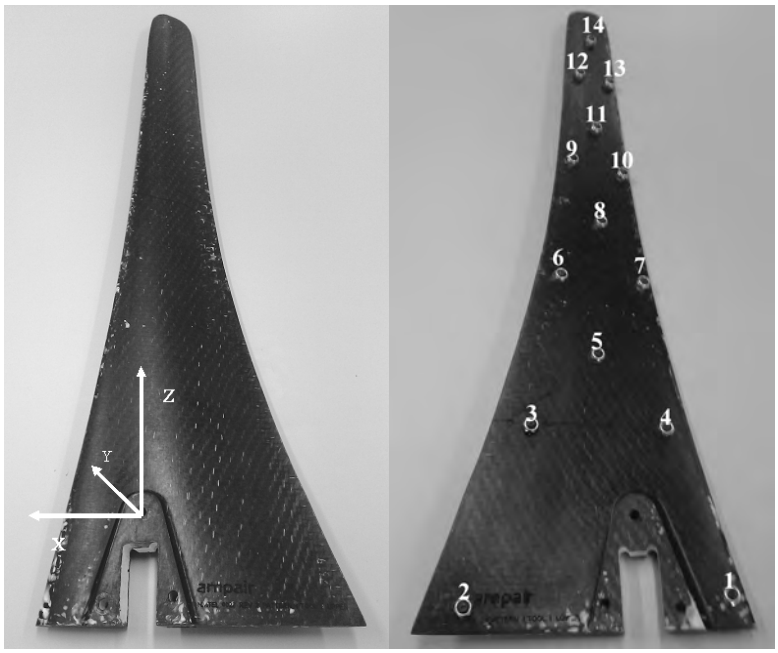

Figure 5-3; Blade global coordinate system and internal measurement points

[1] Julie Harvie et al. [15] have measured six different blades in three different configurations. From the frequency and mode shape correlation it appears that they are comparable and exhibit almost the same dynamic in the tested frequency range. For instance in the free configuration the mean values of the first three modes are ***41.65***, ***124*** and ***188*** [Hz], respectively. The absolute deviations are ***1.46***, ***3.9*** and ***4.7 [Hz]*** which are ***3.5***, ***3.2*** and ***2.8*** percent of the mean values.

The rotational angle of the measurement points, relative to the blade global coordinates are defined using a ***step*** model which is provided by Ampair Energy Ltd. See Table 5-1. The rotation sequence is $\theta=[X, Z]$ and all values are given in degree.

	P_1	P_2	P_3	P_4	P_5	P_6	P_7	P_8	P_9	P_10	P_11	P_12	P_13	P_14
$\Delta\theta_x$	- 3.3	6.9	3.7	- 1.6	0.6	1.78	- 1.1	- 0.2	1	- 0.4	0.0	0.15	- 0.12	0.0
$\Delta\theta_z$	12.9	11.9	17.9	16.7	19	23.4	23.7	23.8	24.5	26	26.6	28.7	28	28

Table 5-1; Local rotational angles at the blade internal measurement points

The blade is mass loaded with a fixture during the measurements which not only provides a mass loading, but also a rigidification of the connection area. The fixture is a chopped off version of the hub joint which is also provided by Ampair Energy Ltd.[1] The fixture (bracket) sandwiches the blade at the root and is attached to the blade using three M-8 bolts which are tightened with ***16 [in-lb]*** as prescribed.[2] Figure 5-4 shows the blade-bracket assembly. Six aluminum blocks are screwed to the bolt end which makes excitation in all three directions possible. See Figure 6-2.

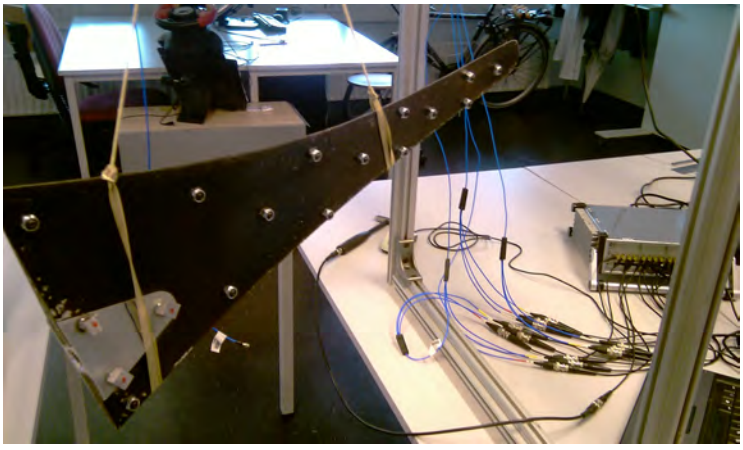

Figure 5-4; Blade hanging free during measurement

The bracket is assumed to have just rigid body dynamic in the frequency range of interest and behave like rigid mass. After measuring the blade-bracket assembly it is subtracted from the model using LM FBS decoupling technique. As consequence the decoupled blade includes the joint stiffness, joint damping and the bolts masses.

[1] We thank Ampair Energy Ltd for providing us the fixtures and the blade drawing.

[2] See Randy L. Mayes [16]

5.2 The Brackets

The bracket is made of aluminum and weights ***0.173 [kg]***. For the use in the decoupling engine the inertia properties and the first elastic mode of it are calculated by mean of a FEM model. This FEM model is validated experimentally.

The principal axes of the bracket are aligned with the global axis of the blade and the moment of inertia about these axis are $I_{xx}=0.1244e^{-3}$, $I_{yy}=0.14e^{-3}$ and $I_{zz}=0.6523e^{-3}$ $[kg.m^2]$ at the bracket center of gravity.

The first elastic mode of the bracket is at ***1700 Hz*** when both bracket lips are flapping. The bracket is pre-stressed in the blade-bracket assembly due to the bolt attachment. So the first elastic mode will be stiffer and its eigenfrequency will shift towards the values above ***1700 Hz***. For this reason the bracket is assumed to behave perfectly rigid up to ***1000 Hz*** and can be treated as lumped mass.

5.3 The Hub

The blades are clamed into the hub joints and together they form the wind turbine rotor which drives the generator inside the nacelle. The hub itself contains a pitch mechanism which adjusts the angle of attack proportional to the wind speed to control the rotational speed. In order to eliminate any nonlinear dynamic such as gapping and rattling the pitch mechanism is fixed using resin mixture. A detailed explanation of the potting procedure is given in Appendix C

After locking the inertia properties are calculated and a full measurement is performed. From the inertia properties the Lumped hub model is raised, based on the theory given in section 4.3. It concerns a model at which the hub is assumed to be perfectly rigid.

The second hub model stems from the full measurement. There is a belief that the low frequency dynamic of the hub-blades assembly is mainly influenced by the mass and inertia of the hub. Considering this, with the benefit of measured inertia properties the best elements out of the full hub measurement are selected and the Full hub model is synthesized.[1] The selection method is very simple and straightforward as it just chose the elements with the closet mass line to that of the lumped model.

Note! Each hub joint has its own local coordinate which are aligned with the global coordinate of the blades. The global coordinate of the blade is shown in Figure 5-3.

[1] See section 6.2 for more details on this

6 Substructures models

The substructures models which are meant for coupling or decoupling aims should be consistent and relatively noise free to avoid spurious peaks and to guaranty accurate results. Realistic measurement configuration comparable to the operational condition will aid to enhance the models and improves the assembly results. Therefore a fixture can be attached to the substructure to load the interface which will be removed analytically after measurement.

In section 3.3 some practical considerations are discussed which benefits the consistency issues during the measurement. They just minimize the inconsistencies and therefore once the data are obtained, the substructure model should be synthesized from the minimum amount of measurement data, to ensure reciprocity and to force symmetry.[1]

For instance just the upper or lower diagonal terms have to be used when a full model is needed. When dealing with CSS the symmetry can be forced by using the symmetry properties and synthesizing the full model as described in section 4.2. This strategy is illustrated schematically in Figure 6-1.

As mentioned in section 5.1 the blade is measured with a fixture attached. At the root (interface) six nodes are fully measured on both ends of the bolts. Three nodes are shown in Figure 6-2 on one side of the blade. To make visualization possible in the subsequent stages, one 3D sensor is roved over fourteen points on the blade. The reference is the first node at the interface. The lower diagonal and all the eighteen driving points are then used to construct the blade model with the fixture attached to it. Hereafter the fixture is subtracted using LM FBS formulation and the final blade model is obtained.

[1] Note! All the models are based on raw measured data and by synthesizing we mean making a model from the minimum amount of data. As we are just using FRF's the term regenerated in the following sections refers to models obtained from modal analysis (synthesis) practices.

The inertia properties of the hub are calculated, employing impact measurement, and are then used to synthesize the lumped hub model. The hub is also fully measured and the full hub model is synthesized from selected FRF's. The selection is based on their mass line.

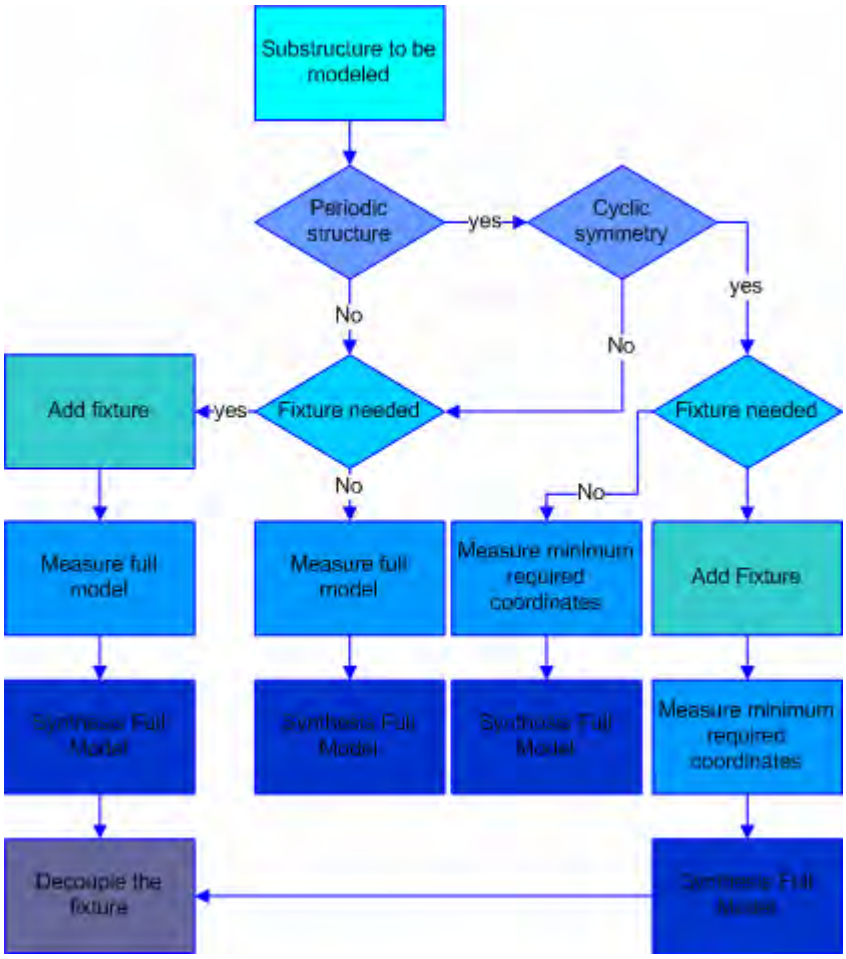

Figure 6-1; Schematic overview of substructure modeling process

This chapter has two sections and gives further details over the blade and hub modeling. Specially is shown how the joint stiffness and damping effects are included in the blade model. In addition, to get more insight in the blade dynamic the first eleven eigenmodes are identified.

At the second section the measured inertia properties are given and an attempt is done to validate them using a checklist and the full hub measurement. Also an explanation is given on how they can be used to examine the quality of the measurement data at the hub interfaces.

6.1 Blade model

In the blade-hub assembly each blade is clamped into one of the hub junctions. The damping at the connection point and the stiffness locally added to the blade due to the joint are not directly measurable and a blade model without them doesn't describe the dynamics of the blade correctly. On way to include the joint stiffness and damping to the blade model is the use of fixture which replicates the actual joint.[1] Measure them together and subtract the fixture from the blade as if it has just inertia. The fixture (bracket) used at the initial blade measurement is shown in Figure 6-2.

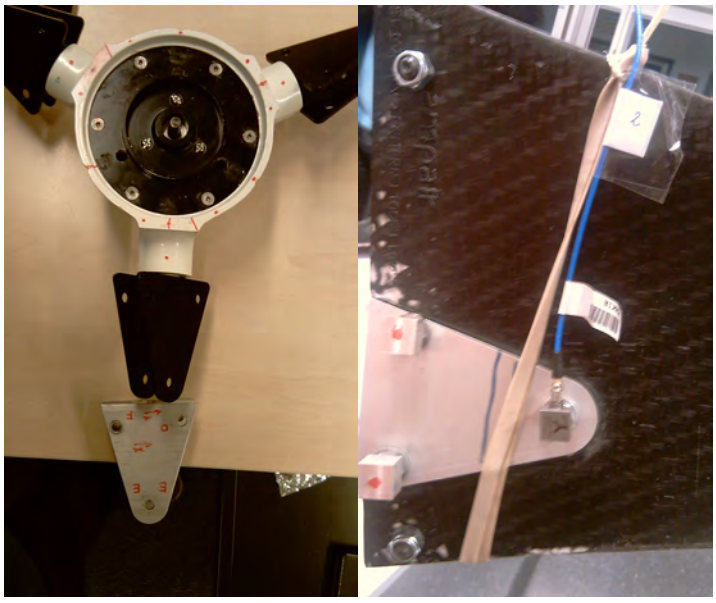

Figure 6-2; Fixture used during blade measurement

To decouple the blade from the bracket the following steps are taken:

- The six nodes at the root, which are fully measured, are mapped into a virtual point using IDM. This virtual point is located at the bracket center of gravity. As such a point is obtained with six DoF's. To apply IDM just the rigid body modes of the fixture are taken into account[2]
- A model of the fixture is made by inverting its mass matrix at its CG.
- Bracket is subtracted form the blade using LM FBS technique

[1] The impedance of the bracket doesn't resemble that of the built-up structure near the connection points as its mass is too small compared to the hub mass but the stiffness which is added locally will be very accurate.

[2] The point at which the blade is decoupled from the fixture will serve as coupling node in the assembly process

Description of the first eleven modes and their eigenfrequencies, before and after decoupling is given in Table 6-1.[1]

		Before decoupling	*After decoupling*
1	**1st bending**	**43.7 [HZ]**	**45.1 [HZ]**
2	**2nd bending**	**121.6 [HZ]**	**125 [HZ]**
3	**1st torsion**	**179.6 [HZ]**	**180.6 [HZ]**
4	**3rd bending**	**235.5 [HZ]**	**241.4 [HZ]**
5	**2nd torsion**	**306.7 [HZ]**	**310.8 [HZ]**
6	**4th bending**	**379.5 [HZ]**	**383.1 [HZ]**
7	**1st edgewise**	**388 [HZ]**	**397.1 [HZ]**
8	**3rd torsion**	**472.4 [HZ]**	**476.2 [HZ]**
9	**5th bending**	**566.9 [HZ]**	**567.8 [HZ]**
10	**4th torsion**	**633.8 [HZ]**	**639.5 [HZ]**
11	**6th bending**	**736.8 [HZ]**	**736.4 [HZ]**

Table 6-1; Blade natural frequencies, before and after decoupling

Subtracting the mass from the blade changes the modal masses and with that all modal eigenfrequencies. To validate the blade model the fixture is removed and the blade is measured at the root without removing the bolts and screws. In Figure 6-3 one driving points is shown before and after decoupling with the validation.

Comparing the solid line with the dashed line one sees that the average amplitude of the response is greater and the resonances are shifted to the right as a result of mass removal.[2] Also more modes are absorbed and are identifiable which means that the boundary condition is more realistic compared to the operational condition of the structure and that the fixture works the blade locally. The difference between the dotted (validation) and the dashed (blade decoupled) line shows that the fixture doesn't just has mass loading effect but also add stiffness and damping to the system. For instance the 1st torsion, the 1st edgewise and 3rd torsion are less stiff without the bracket and their resonance are shifted to left instead of being shifted to right like the bending modes.

[1] All the modes are visualized in Appendix A.

[2] The average amplitude of each FRF is greater because the mass lines are shifted upwards

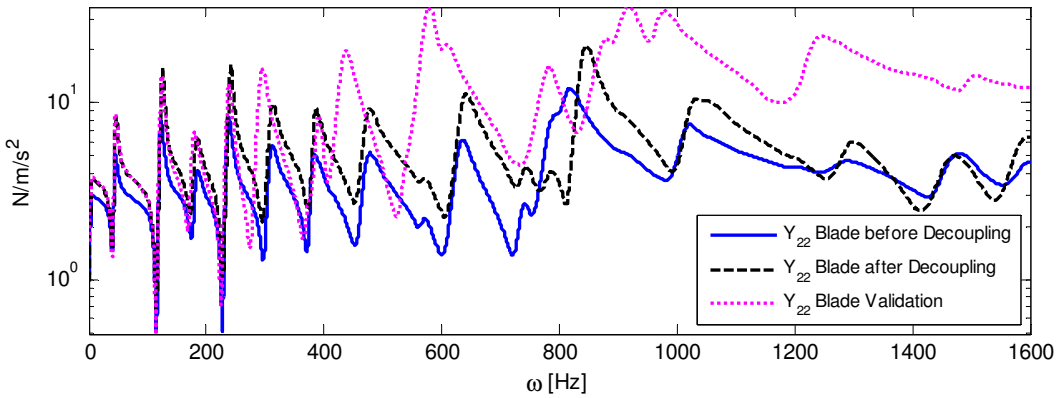

Figure 6-3; Blade validation after decoupling

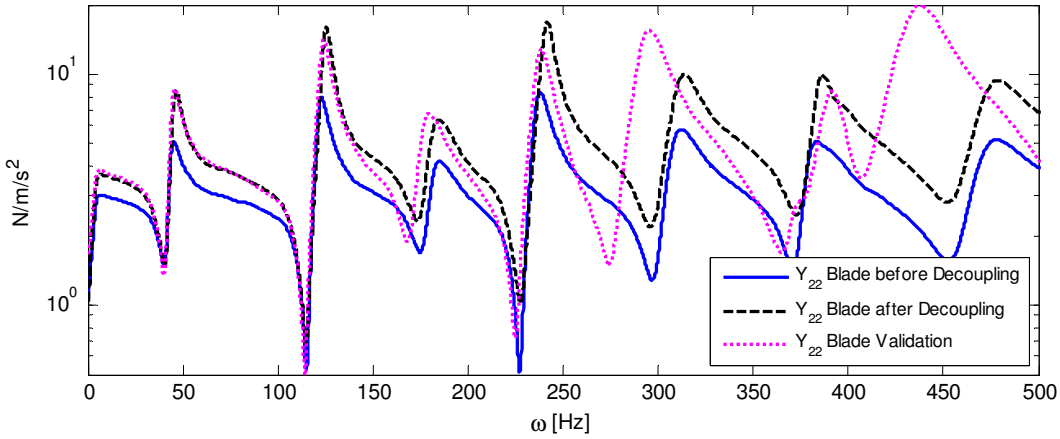

Figure 6-4; Blade validation after decoupling up to 500 [Hz]

For the blades two models are made. The first model is obtained after applying decoupling to the raw measured data. The second model is made after applying decoupling to the regenerated data which is obtained after experimental modal analysis.[1]

6.2 Hub models

The hub is measured two times and two hub models exist. One model describes the hub as it is measured at the interfaces (Full Model) and the second model as it behaves like a rigid mass (Lumped Model).[2] Figure 6-5 shows the measurement configuration of the hub. Three points at each junction are measured in contrast with the blade where all six points are measured.

[1] To regenerate the blade measurement, eighteen modes are indentified up to ***1600 Hz***. The lower and upper residuals are also taken into account.

[2] The measured inertia properties have assist to make a selection between the measured coordinates in order to make a full model of the hub.

Figure 6-5; Hub hanging free during measurement

According to Eq. (4.11) the full hub model can be obtained if two matrix blocks, $\boldsymbol{Y_{AA}}$ and $\boldsymbol{Y_{AB}}$ are known. $\boldsymbol{Y_{AA}}$ is the full FRF of one joint and $\boldsymbol{Y_{AB}}$ is the full FRF measured from one joint to another joint.[1]

The inertia properties of the hub can be obtained if a proper 3D-drawing of the hub exists. But immeasurable components like the pitch mechanism and the bearings on one hand and the unknown material properties and undefined geometrical shape of the molded epoxy on the other hand making 3D-modelling very complicated and time consuming.

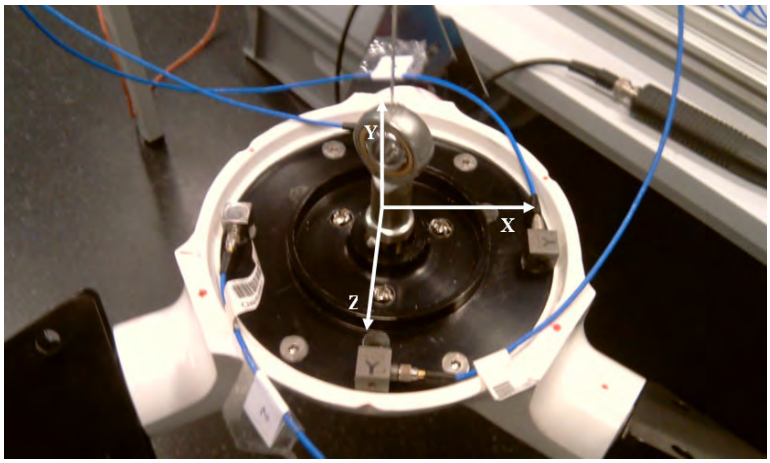

Figure 6-6; Hub hanging free during inertia property measurement

As result the hub inertia is preferably measured. To accomplish this task four 3D-acceleration sensors are attached to the hub as shown in Figure 6-6 and six impact measurements are carried out. Applying Eq. (3.8) and (3.9) successively to the measured data from ***10*** to ***24 [Hz]*** the inertia values are obtained which are given in Table 6-2.

[1] Using these two blocks to synthesize the full hub model will ensure the reciprocity.

	m	x_{og}	y_{og}	z_{og}	$J_{xx}{}^{o}$	$J_{xy}{}^{o}$	$J_{xz}{}^{o}$	$J_{yy}{}^{o}$	$J_{yz}{}^{o}$	$J_{zz}{}^{o}$
Hub-I.P.	**3.85**	**0.0014**	**- 0.0386**	**0.0**	**0.0201**	**0.0003**	**- 0.0002**	**0.0288**	**0.0004**	**0.0212**

Table 6-2; Hub Inertia properties

These values are measured for a virtual point located at rotational axis of the hub on the same plane where the sensors are attached to the hub. The local coordinates are aligned such that one of the axes is directed in the same direction as the rotation axis of the hub.

The calculated mass is exact the same mass as the hub would have on the scale. To examine whether the other results are correct the following point could be checked:[1]

- The hub is axisymmetric, so $\boldsymbol{J_{xx}{}^{o}}$ should equals $\boldsymbol{J_{yy}{}^{o}}$ and the products of inertia should be close to zero.[2]
- The rotational axis is a principal axis and the distance of any point on this axis to the center of gravity is described by just one coordinate. So $\boldsymbol{x_{og}}$ and $\boldsymbol{y_{og}}$ both should be very close to zero unless the hub is poorly balanced.
- The moment of inertia should be highest around the rotational axis (topspin axis).

Looking at the values given in Table 6-2 one may conclude that we pass the checks. One another way to examine the results is to compare the lumped hub model with the full hub measurement. The synthesized results at the hub joint should resemble the mass lines of the full hub measurement. Figure 6-7 illustrates this idea.

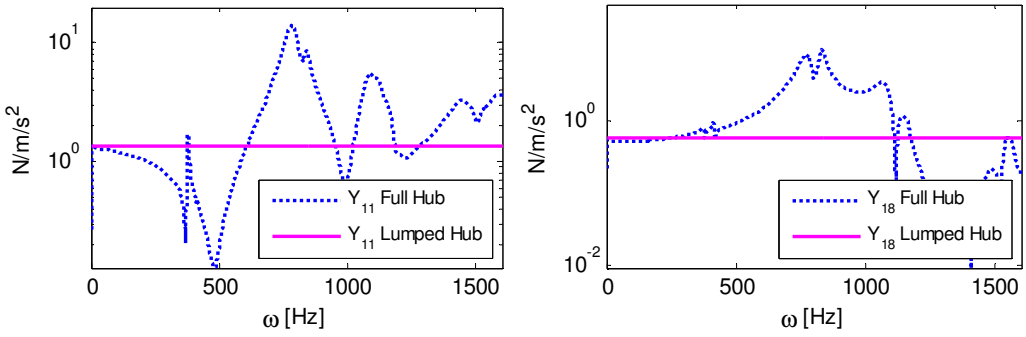

Figure 6-7; Comparison lumped hub model with full hub measurement

[1] These checks might also be used as boundary condition during the calculations. For instance mass can be used to select the frequency range.

[2] The product of inertia can be positive, negative or zero and are a measure of imbalance in the mass distribution.

To check the entire model a tool is utilized which is known as Frequency Response Assurance Criterion (FRAC). FRAC-number is comparable with MAC-number and for two FRF's, Y_a and Y_b, in the frequency range of $\omega_1 \leq \omega \leq \omega_2$, is given with:[1]

$$FRAC = \frac{\left(\left| \sum_{\omega=\omega_1}^{\omega_2} Y_a Y_b^* \right| \right)^2}{\left| \sum_{\omega=\omega_1}^{\omega_2} Y_a Y_a^* \right| \left| \sum_{\omega=\omega_1}^{\omega_2} Y_b Y_b^* \right|} \tag{6.1}$$

For the frequency range of *40* to *60 Hz* FRAC-number is given in Figure 6-8. From the *324* FRF's, *286* FRF's resemble the mass line of the full measurement, above *95%*. X, Y, Z, θ_X, θ_Y and θ_z are the six coupling coordinates. With this result the calculated inertia properties are approved one more time.

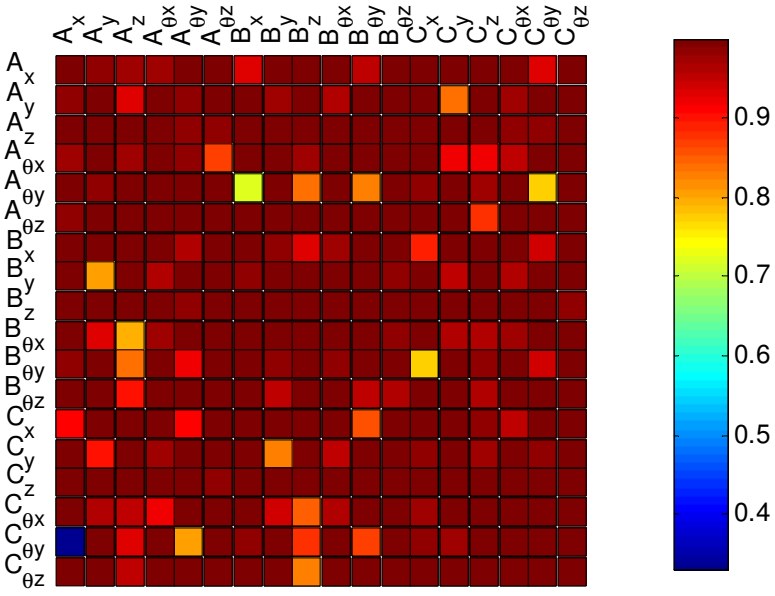

Figure 6-8; FRAC relating lumped hub model to full measurement from *40 to 60 Hz*

The lumped hub model can also be used as a reference to choose the best FRF's out of the full hub measurement in order to synthesis the full hub model as we just need two block matrices. See Eq. (4.11) for clarity. However the coupling is going to be performed

[1] See Randall J. Allemang [16]

from frequencies lower than ***40 Hz***. Computing FRAC from ***10*** to ***60 Hz*** gives very different picture; Just ***73*** FRF's are in accordance above ***95%***, ***118*** above ***90%*** and ***203*** above ***80%***. See Figure 6-9. It shows how difficult it is to measure the hub in low frequency region and that data should be checked twice.

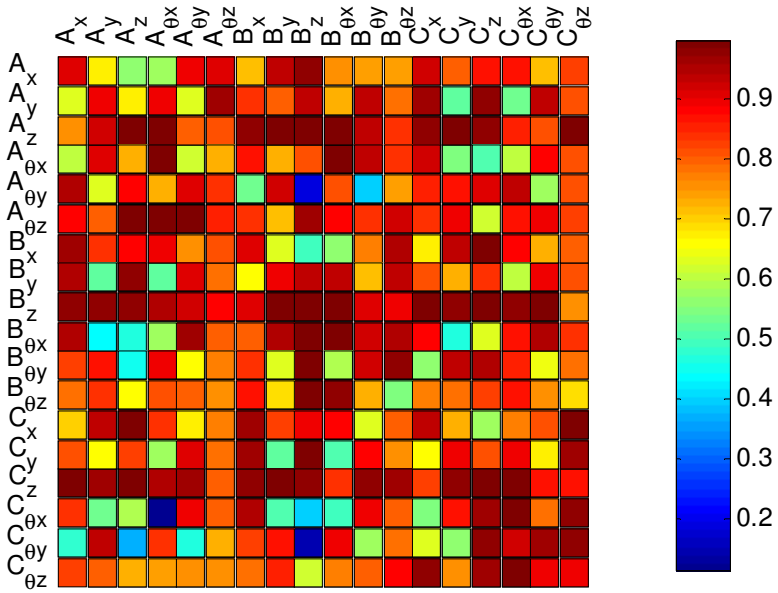

Figure 6-9; FRAC relating lumped hub model to full measurement from *10 to 60 Hz*

The block matrices $\boldsymbol{Y}_{AA}$, $\mathbf{Y}_{\mathrm{CC}}$ or even $\boldsymbol{Y}_{BB}$ can be used to form $\boldsymbol{Y}_{AA}$. Once one of them is chosen the main diagonal plus the lower or upper diagonal might be used to form the $\boldsymbol{Y}_{AA}$. It is also possible to select the best element out of $\boldsymbol{Y}_{AA}$ by comparing the upper and lower diagonal and use the best FRF to synthesis the $\boldsymbol{Y}_{AA}$.

To select the $\boldsymbol{Y}_{AB}$ or $\boldsymbol{Y}_{BA}$ one of the off diagonal sub matrices could be selected. The selection can be based on the sum of the FRAC-numbers over the sub matrices.

7 Assembly and Validation

As discussed in the pervious chapters blade and hub both are experimentally modeled. These models are going to be assembled in this chapter. From the blade measurement two blade models are deduces. One is pure based on raw measured data and the other on the regenerated data. Hub is modeled twice. One model is based on the inertia properties while the other model is formed directly from the test data.

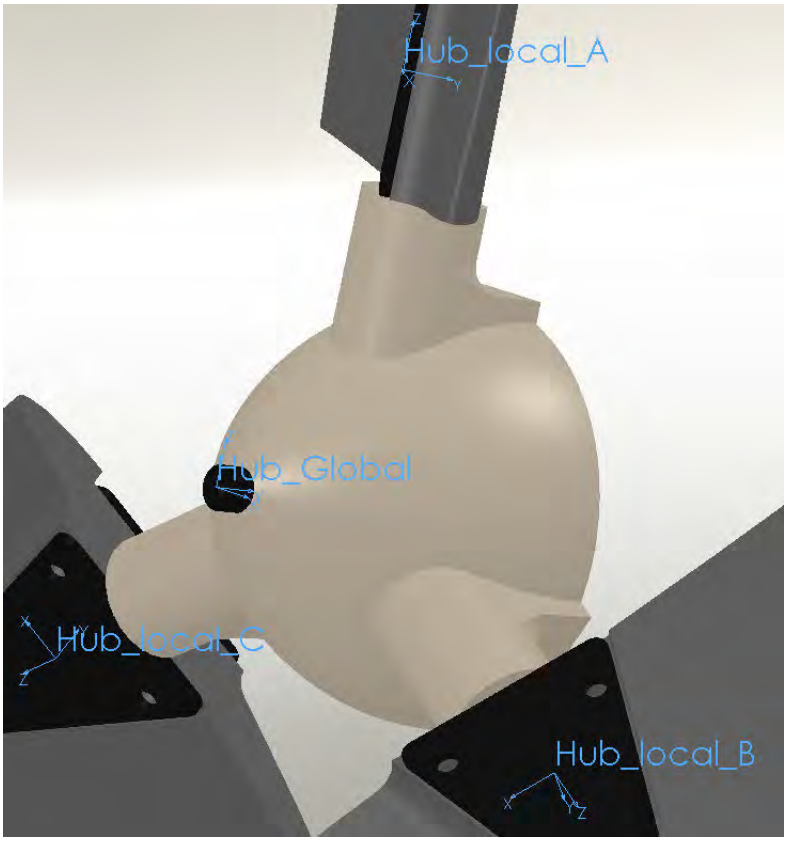

Figure 7-1; Local and global coordinates of the hub

The assembly consists of three identical blades and the hub and the assembly is performed through three coupling nodes in the locale coordinates of the joints.[1] To make the visualization of the modes possible, fourteen internal points on the blade are measured and are involved in the coupling procedure.

The global coordinates of the blades coincide with the local coordinates of the hub. When coupling is done the results are transformed to the global direction and the modes are extracted. In Figure 7-1 the local and global coordinates are given.

In this chapter first the assembly procedure is highlighted and the four coupling variants are defined. Then the results are validated and the best two are discussed, studied and evaluated further. Thereafter the mode shapes are identified and illustrated for both variants. This chapter finishes with discussion and comparison of the obtained mode shapes.

[1] Each node has six DoF's

7.1 Coupling procedure and coupling variants

The coupling start with placing the uncoupled substructure models as block matrices on the main diagonal of the uncoupled assembly matrix $\boldsymbol{Y}$ as describe by Eq. (2.24):

$$Y = \begin{bmatrix} Y^{H}_{c_1c_1} & Y^{H}_{c_1c_2} & Y^{H}_{c_1c_3} & 0 & 0 & 0 & 0 & 0 & 0 \\ Y^{H}_{c_2c_1} & Y^{H}_{c_2c_2} & Y^{H}_{c_2c_3} & 0 & 0 & 0 & 0 & 0 & 0 \\ Y^{H}_{c_3c_1} & Y^{H}_{c_3c_2} & Y^{H}_{c_3c_3} & 0 & 0 & 0 & 0 & 0 & 0 \\ 0 & 0 & 0 & Y^{B^1}_{cc} & Y^{B^1}_{ci} & 0 & 0 & 0 & 0 \\ 0 & 0 & 0 & Y^{B^1}_{ic} & Y^{B^1}_{ii} & 0 & 0 & 0 & 0 \\ 0 & 0 & 0 & 0 & 0 & Y^{B^2}_{cc} & Y^{B^2}_{ci} & 0 & 0 \\ 0 & 0 & 0 & 0 & 0 & Y^{B^2}_{ic} & Y^{B^2}_{ii} & 0 & 0 \\ 0 & 0 & 0 & 0 & 0 & 0 & 0 & Y^{B^3}_{cc} & Y^{B^3}_{ci} \\ 0 & 0 & 0 & 0 & 0 & 0 & 0 & Y^{B^3}_{ic} & Y^{B^3}_{ii} \end{bmatrix} \tag{7.1}$$

where $\boldsymbol{H}$, $\boldsymbol{B^1}$, $\boldsymbol{B^2}$ and $\boldsymbol{B^3}$ stand for ***Hub***, ***Blade-1***, ***Blade-2*** and ***Blade-3***, respectively. To apply LM FBS to Eq. (7.1) first the Boolean matrix should be defined as:

$$B = \begin{array}{c} \begin{matrix} H_{c1} & H_{c2} & H_{c2} & B^1{}_c & B^1{}_i & B^2{}_c & B^2{}_i & B^3{}_c & B^3{}_i \end{matrix} \\ \begin{bmatrix} I & 0 & 0 & -I & 0 & 0 & 0 & 0 & 0 \\ 0 & I & 0 & 0 & 0 & -I & 0 & 0 & 0 \\ 0 & 0 & I & 0 & 0 & 0 & 0 & -I & 0 \end{bmatrix} \end{array} \begin{matrix} H_{c1} \\ H_{c2} \\ H_{c3} \end{matrix} \tag{7.2}$$

where $\boldsymbol{c_1}$, $\boldsymbol{c_2}$ and $\boldsymbol{c_3}$ are the unique coupling coordinates. The coupled assembly matrix will look like:

$$Y_{tot} = \begin{bmatrix} Y_{c_1c_1} & Y_{c_1c_2} & Y_{c_1c_3} & Y_{c_1c_1} & Y_{c_1b_1} & Y_{c_1c_2} & Y_{c_1b_2} & Y_{c_1c_3} & Y_{c_1b_3} \\ Y_{c_2c_1} & Y_{c_2c_2} & Y_{c_2c_3} & Y_{c_2c_1} & Y_{c_2b_1} & Y_{c_2c_2} & Y_{c_2b_2} & Y_{c_2c_3} & Y_{c_2b_3} \\ Y_{c_3c_1} & Y_{c_3c_2} & Y_{c_3c_3} & Y_{c_3c_1} & Y_{c_3b_1} & Y_{c_3c_2} & Y_{c_3b_2} & Y_{c_3c_3} & Y_{c_3b_3} \\ Y_{c_1c_1} & Y_{c_1c_2} & Y_{c_1c_3} & Y_{c_1c_1} & Y_{c_1b_1} & Y_{c_1c_2} & Y_{c_1b_2} & Y_{c_1c_3} & Y_{c_1b_3} \\ Y_{b_1c_1} & Y_{b_1c_2} & Y_{b_1c_3} & Y_{b_1c_1} & Y_{b_1b_1} & Y_{b_1c_2} & Y_{b_1b_2} & Y_{b_1c_3} & Y_{b_1b_3} \\ Y_{c_2c_1} & Y_{c_2c_2} & Y_{c_2c_3} & Y_{c_2c_1} & Y_{c_2b_1} & Y_{c_2c_2} & Y_{c_2b_2} & Y_{c_2c_3} & Y_{c_2b_3} \\ Y_{b_2c_1} & Y_{b_2c_2} & Y_{b_2c_3} & Y_{b_2c_1} & Y_{b_2b_1} & Y_{b_2c_2} & Y_{b_2b_2} & Y_{b_2c_3} & Y_{b_2b_3} \\ Y_{c_3c_1} & Y_{c_3c_2} & Y_{c_3c_3} & Y_{c_3c_1} & Y_{c_3b_1} & Y_{c_3c_2} & Y_{c_3b_2} & Y_{c_3c_3} & Y_{c_3b_3} \\ Y_{b_3c_1} & Y_{b_3c_2} & Y_{b_3c_3} & Y_{b_3c_1} & Y_{b_3b_1} & Y_{b_3c_2} & Y_{b_3b_2} & Y_{b_3c_3} & Y_{b_3b_3} \end{bmatrix} \tag{7.3}$$

The coupled assembly matrix $\boldsymbol{Y_{tot}}$ contains redundant FRF's like $\boldsymbol{Y_{c1c1}}$ and not measured FRF's like $\boldsymbol{Y_{b1b1}}$. Squeezing Eq. (7.3) in order to get rid of them gives the final coupled assembly matrix:

$$Y_{tot} = \begin{bmatrix} Y_{c_1c_1} & Y_{c_1c_2} & Y_{c_1c_3} \\ Y_{c_2c_1} & Y_{c_2c_2} & Y_{c_2c_3} \\ Y_{c_3c_1} & Y_{c_3c_2} & Y_{c_3c_3} \\ Y_{b_1c_1} & Y_{b_1c_2} & Y_{b_1c_3} \\ Y_{b_2c_1} & Y_{b_2c_2} & Y_{b_2c_3} \\ Y_{b_3c_1} & Y_{b_3c_2} & Y_{b_3c_3} \end{bmatrix} \tag{7.4}$$

For each substructure two models are available which make four combinations possible. These four combinations are:

1. regenerated blade-lumped hub (RBL)
2. regenerated blade-full hub (RBF)
3. measured blade-lumped hub (MBL)
4. measured blade-full hub (MBF)

7.2 Validation

To validate the results the blades are connected to the hub and a full measurement is carried out. The bolts are tighten with $\boldsymbol{16\ [in\text{-}lb]}$ and the hub is hanging free as a pendulum and at each hub junction three points are measured in three directions. Measurement points are identifiable with the aluminum blocks as shown in Figure 7-2. Aluminum blocks are used as dummy masses as the sensors needed to be roved.

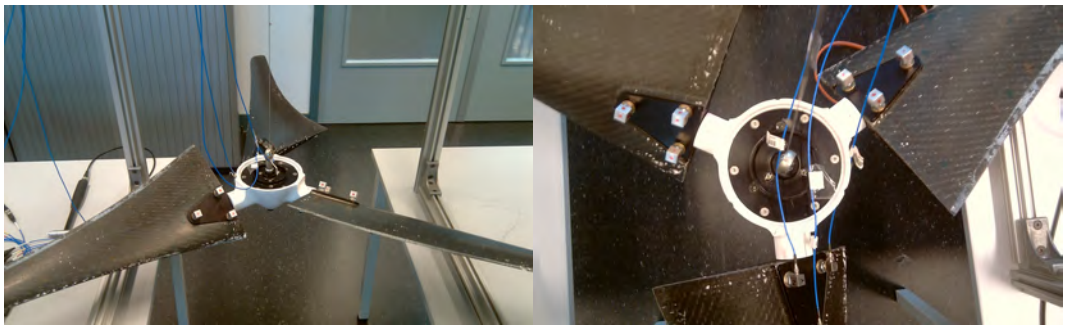

Figure 7-2; Hub-blades assembly hanging during validation measurement

To compare the coupling results with the validation Complex Mode Indicator Function (CMIF) is employed.[1] CMIF indicates the existence of real and complex modes.

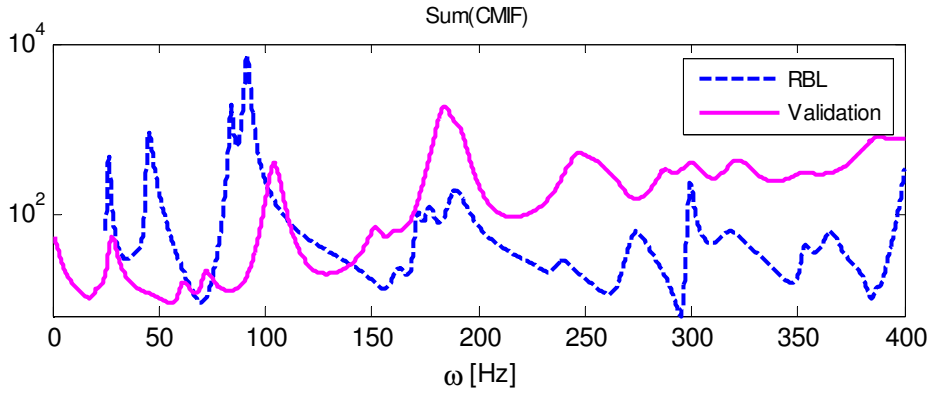

Figure 7-3; Sum over the RBL's CMIF curves

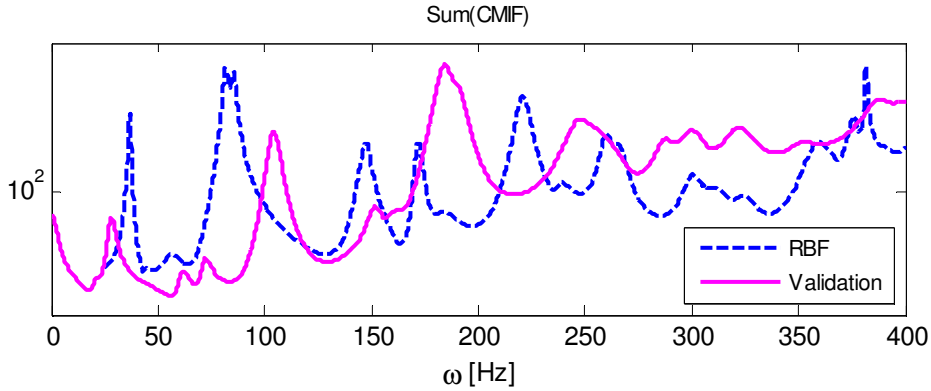

Figure 7-4; Sum over the RBF's CMIF curves

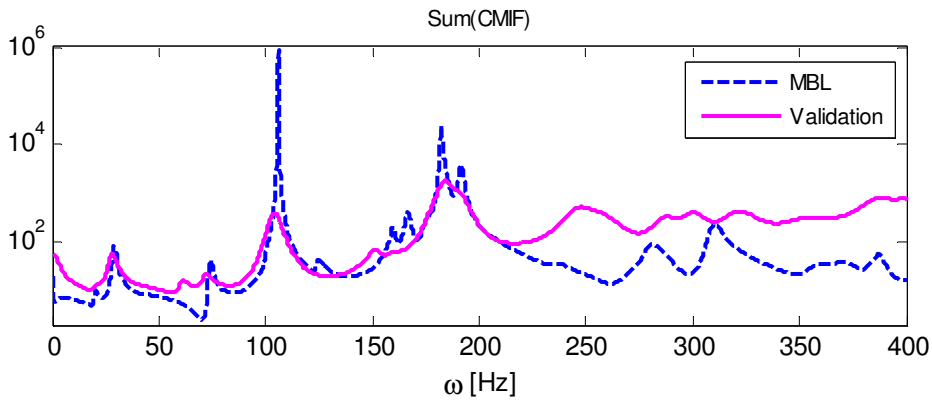

Figure 7-5; Sum over the MBL's CMIF curves

[1] Number of CMIF plots equals the driving point measurements.

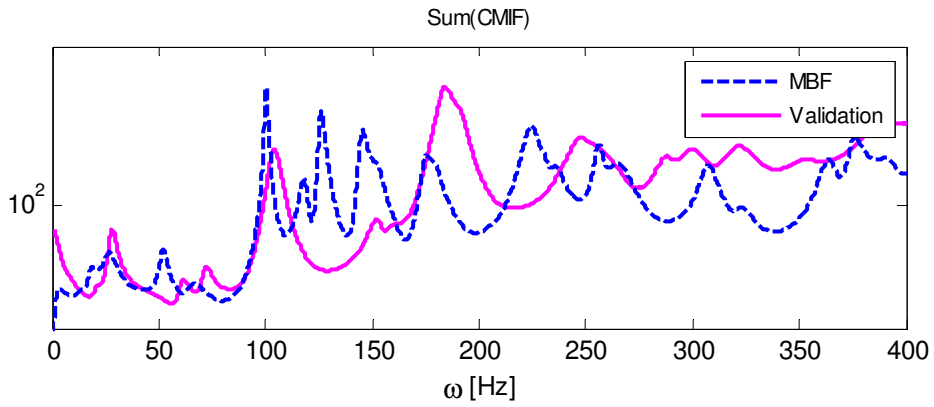

Figure 7-6; Sum over the MBF's CMIF curves

The peaks in the CMIF plot represent modes and their corresponding frequency, and consequently it can be use to examine the quality of the obtained results and check if spurious peaks are present in the prediction. Figure 7-3 through Figure 7-6 show the sum of CMIF curves for all four coupling variants together with that of the validation. Agreement between the validation and assembly results serve as an indicator of the coupling correctness and quality, so one may conclude:

- The *RBL* shows remarkable inaccurate predictions and is poor both in low frequency and high frequency region
- The *RBF* results are slightly better but aren't accurate and don't predict the reality
- In contrast to *RBL*, the overall *RBF* amplitude at high frequency region looks more like the validation which is caused by **not** neglecting the elastic modes of the hub.

In general one may state that the predicted natural frequencies of *RBL* and *RBF* are wrong and the average amplitude doesn't always match. These can be the results of the regenerated blade model and confirms that it doesn't describe the blade reasonable and is not feasible. It might be caused by:

- damping which is distributed in a non proportional way[1]
- close modes
- the absence of proper lower and higher residual terms
- too complex higher modes
- not uncoupled modes due to complex damping mechanism

In contrast to *RBL* and *RBF*, *MBL* and *MBF* give much better results and have a very close characteristic to that of the validation. Especially *MBL*, where hub is modeled

[1] For instance the damping in the joint is not distributed proportional.

rigidly, estimates the lower frequency region very accurately. But same as *RBL* the overall response amplitude at higher frequencies is overestimated. See Figure 7-5. It shows nine resonances up to ***185 Hz***, from which some are in perfect accordance with the validation. It miss a resonance at ***60 Hz*** and exhibits between ***100*** and ***180 Hz*** more peaks than are present in the validation.

MBF also produce reliable results but prediction at the lower region is not good as *MBL*. However the average amplitude at the higher region improves. It predicts more resonances but unlike the *MBL* misses no peaks. See Figure 7-6.

In Figure 7-7 a driving point and a cross point, from one blade to another blade, of both models, *MBL* and *MBF* are visualized. It appears that the lumped hub results are still very reliable up to 200 Hz and full hub model improves the assembly prediction at the higher frequency range.

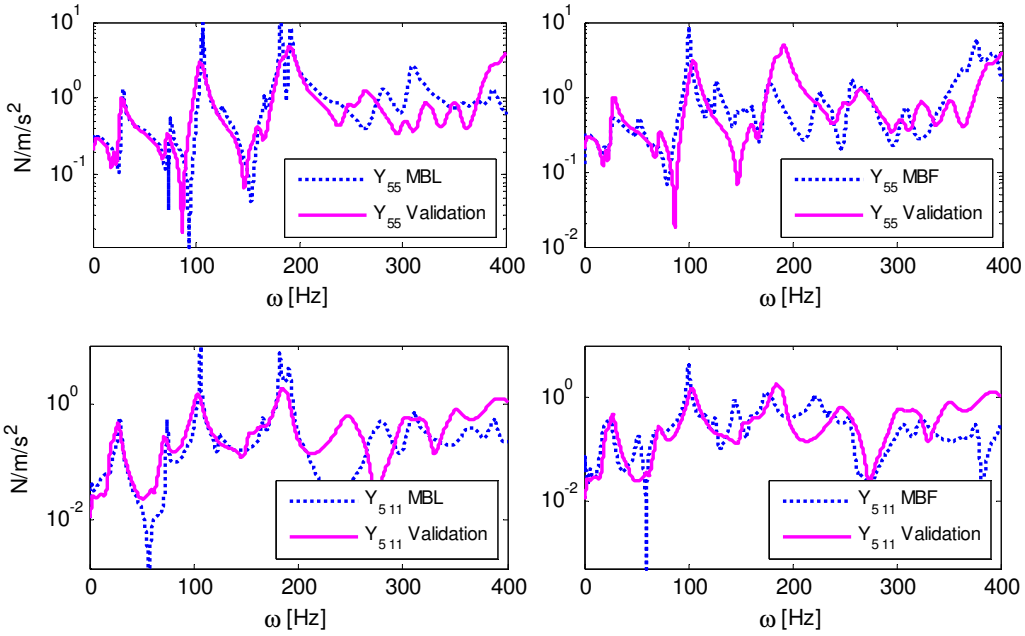

Figure 7-7; Typical driving point/cross FRF pertain to MBF and MBL with the validation of coupled structure

It can be concluded that the regenerated blade doesn't improve the assembly prediction and shouldn't be used.[1] The blade, as it is measured, produces with both hub models proper results. Assemblies, *MBL* and *MBF* will be further studied, the eigenmodes will be identified and the nature of them will be investigated.

[1] It might illustrate the value of experimental DS in general as experimental modal analysis seems not adequate to analyze the coupling.

7.3 Discussion

To investigate the nature of the peaks and to compare the *MBL* with *MBF*, the associated mode shapes of both coupling variants are identified. Studying the mode shapes possibly will help to understand the nature of the present peaks. Are they spurious peaks and are the product of inconsistent models or/and noise? Or are they associated with the modes which are not excited properly during the validation?

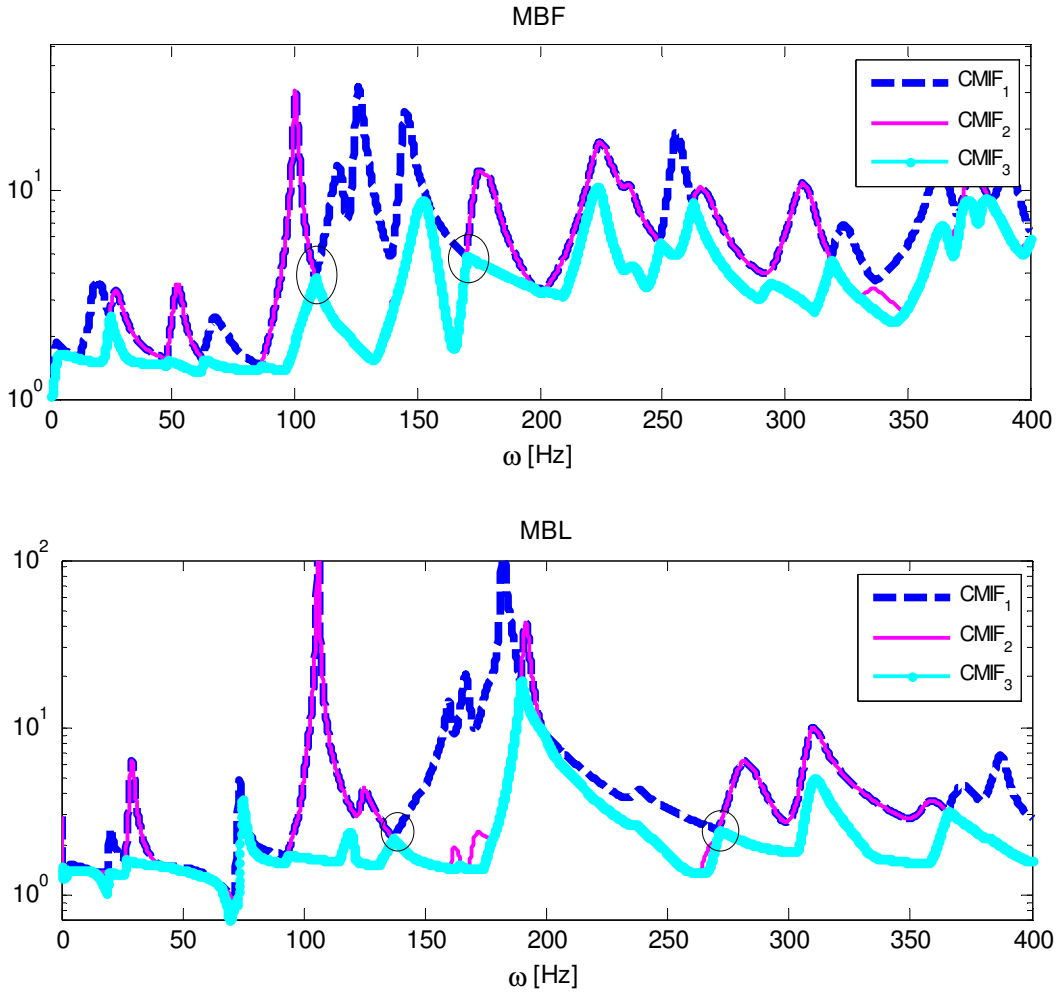

Figure 7-8; Highest CMIF curves pertain to MBF and MBL, respectively

Figure 7-8 shows the first three largest CMIF plots of both assemblies. The peaks which are encircled are apparent peaks and don't belong to structural resonances. They are due to the way the CMIF is plotted. CMIF is defined as singular values plotted as a function of frequency. Number of CMIF plots equals the driving point measurements. The largest eigenvalue is plotted first followed by smaller eigenvalues. Since the contribution from different modes varies along the frequency line, at a specific frequency the contribution of two modes can be almost the same. At this frequency these eigenvalue

curves cross each other and the lower curve appears to a peak while the higher eigenvalue appears to a dip.[1]

In the lower frequency range up to ***185 Hz***, *MBL* has 9 modes and for MBF 10 modes are identified. All the modes are visualized and given in Appendix B. Not considering the *MBF* 3rd mode, comparing *MBL* with *MBF*, all modes exhibit approximately the same nature. The natural eigenfrequency and modal damping of all modes are given in Table 7-1.

	MBF		**MBL**	
1st mode	**18.8 [Hz]**	**15.64 %**	**20.9 [Hz]**	**4.4 %**
2nd mode	**25.4 [Hz]**	**8.1 %**	**29.0 [Hz]**	**3.5 %**
3rd mode	**52.3 [Hz]**	**3.41 %**	**n/a**	**n/a**
4th mode	**65.5 [Hz]**	**0.15 %**	**74.3 [Hz]**	**1.1 %**
5th mode	**98.3 [Hz]**	**-0.55 %**	**106.4 [Hz]**	**0.2 %**
6th mode	**117.0 [Hz]**	**1.00 %**	**118.0 [Hz]**	**2.4 %**
7th mode	**125.0 [Hz]**	**0.23 %**	**123.8 [Hz]**	**8.1 %**
8th mode	**144.3 [Hz]**	**1.43 %**	**159.4 [Hz]**	**2.4 %**
9th mode	**151.6 [Hz]**	**0.86 %**	**167.6 [Hz]**	**0.5 %**
10th mode	**178.8 [Hz]**	**1.19 %**	**182.4 [Hz]**	**1.65 %**

Table 7-1; Eigenfrequency and modal damping of extracted modes

The 1st mode is flapping mode at which all blades are flapping in the same direction as they have been clammed at the root and show their first bending mode. They are all in phase. The 2nd mode is also flapping mode but two blades are in phase and one is out of phase. This mode is a double mode as two CMIF curves have high values. [2]

The 3rd and 4th modes are the second flapping modes which are related to the second bending mode of the blades being clammed. In the 3rd *MBF* and 4th *MBL* mode two blades are flapping in phase while the third one is out of phase. This mode is also double. In the 4th *MBF* mode all blades are flapping in phase. *MBL* doesn't predict this mode.

[1] See Allyn W. Phillips et al. [18]

[2] The blades attached to the hub behave like being clammed at interface as their mass compared to that of the hub is smaller. The bending modes in this configuration are quite different from the bending modes of the blade which are given in appendix A and measured in free configuration.

From the 5th mode begins the third group of modes which are associated to the third bending mode of the blade. The *MBL* 5th mode exhibits some kind of traveling waves where the blades bend after each other cyclically. This mode is also a double mode as the traveling wave could be a sine or a cosine. At the *MBF* 5th modes two blades are bending out of phase while the third blade stands approximately still. The modal damping values for both cases are very remarkable. It is too low for *MBL* and even negative for *MBF*.

The *MBF* 6th and 7th modes are the modes at which all blades are bending in phase. Both exhibit approximately the same overall shape but locally they are slightly different. For the *MBL* holds that at the 6th mode all blades are in phase and at the 7th mode one blade is out of phase and consequently the 7th mode is a double mode.

8th and 9th modes for both assemblies are complex and the first torsion mode of the blades start to appear on top of the third bending mode. At the *MBF* 9th mode one of the blades is twisting while the other two are bending. This mode is a double mode. At the 8th *MBF*, 8th and 9th *MBL* modes all blades are bending and also twisting at the same time and are all in phase.

The 10th mode for both assemblies is the pure torsion mode where the blades twist. At the 10th *MBF* mode one blade is twisting out of phase which makes this mode a double mode. At the 10th *MBL* mode all blades are twisting in phase.

One notable issue is the modal damping of some modes which are too low. This may have been caused by the joint damping in the assembled system which differs from the joint damping included in blade model. The fixture mass is not comparable to the hub mass which can cause different damping mechanism and with that different modal damping for certain modes.

One another remarkable thing is the negative modal damping of the 5th MBF mode. The real part of the driving point FRF's are correct as they first go trough their minimum before they pass the zero line. Also the imaginary parts are investigated and all of them are negative while for driving point they should be all positive. It causes the Nyquist plot to rotate in the counter clock direction which may result in negative damping identification.

8 Conclusion and Recommendations

To Advance and categorize the experimental DS technology and theory and compare the existing methods a test bed is initiated by Society of Experimental Mechanics substructuring subgroup. As a member, the Engineering Dynamic workgroup at Delft University of technology takes part in this program by putting his knowledge into practice and developing new methods for successful and efficient experimental DS.

The research topics treated in this thesis are related to experimental substructure modeling, coupling and decoupling, applied to the test bed and will aid to fulfill the thesis assignment objective:

"Apply Lagrange Multiplier Frequency Based Substructuring (Coupling/Decoupling) to the 600 Ampair wind turbine in order to accomplish the first iteration by assembling the blades with the hub"

In this work first FBS is introduced followed by LM FBS for both coupling and decoupling. Then typical issues pertaining to experimental DS such as rigid body dynamic, coordinate incompleteness, noise and inconsistency are highlighted. It is shown how to rigidify the interface in order to obtain rotational DoF's and how inertia properties could be measured directly from impact measurements.

All measurements are carried out in free configuration and some structures are mass loaded during the measurements with a fixture. The fixture works the substructure locally and gives a better representation of reality. By means of LM FBS decoupling technique the fixture is then removed from the substructure model as if it is rigid.

Regarding the Cyclic Symmetric Structures (CSS) two methods are proposed to model them. The first method is namely developed to synthesis the CSS full model from the minimum number of measured coordinates. It uses the fact that the Inertance

(Receptance, Mobility or Accelerance) matrix is circulant and by cyclic permuting of one column the other columns might be obtained.

The second method describes, knowing the inertia properties, how to lump the CSS and get the inertance at any given point. It uses the inertance at a given point, in respect to which the inertia properties are given\calculated, and by mean of geometrical relations calculate the inertance at any other point. Both methods produce experimental models which are defined in the local coordinates of the interface nodes.

In this chapter first the blade and hub modeling steps are described briefly followed by some findings during the modeling process. All the models are synthesized from the minimum amount of measurement data, to ensure reciprocity and to force symmetry. Hence they not just a set of compiled data. It results in two blade and two hub models. Then the four possible assembly results are discussed and evaluated. This chapter ends with recommendations which content the questions left unanswered.

8.1 Conclusion

The Ampair 600 wind turbine consists of three blades, hub, nacelle, tower and the base which is supported on a trampoline. See Figure 5-1. Delft University of Technology has decided to initiate the first iteration by substructuring the hub and three blades. In Figure 5-2 the assembly is shown which is used to validate the synthesized hub-blades model.

One blade is modeled and used three times in the hub-blades assembly. The blade is measured with a fixture which is assumed to be rigid in the frequency range of interest. Six interface nodes and fourteen internal nodes are measured and the blade-fixture assembly is obtained. The blade-fixture assembly is also regenerated. Using raw measured data and regenerated data then the blade is decoupled from the fixture and consequently two blade models are constructed. The fixture is modeled analytically. The blade has ***11*** modes up to ***740 [Hz]***, ***6*** are flap wise bending, ***4*** torsion and ***2*** edge wise bending modes. After removing the fixture the following has been absorbed:

- the average amplitude of each FRF is greater because the mass lines are shifted upwards as consequence of a lighter structure
- the resonances are shifted to right as a result of mass removal
- in the frequency range of interest more modes are absorbed and are identifiable
- fixture doesn't just mass loads the interface but also rigidifies the connection area. For instance the 1^{st} torsion, 1^{st} edgewise and 3^{rd} torsion modes are more stiff with the bracket and their resonance are shifted to left instead of being shifted to right

For the hub also two models are constructed. One model describes the hub as it is measured at the interfaces (Full Model) and the second model as it behaves like a rigid mass (Lumped Model). To form the lumped model the inertia properties are needed which are measured directly from impact measurement using four acceleration sensors. The results are checked for correctness and are justified. The measured values are given in Table 6-2.

The lumped hub model is also used to select the best FRF's from the fully measured hub. In the low frequency region the dynamic of the blade-hub assembly is dictated by the mass of the hub. So the best measured FRF's are the one with the closest mass line to that of the lumped model. When comparing the fully measured hub with the lumped hub model it can be concluded that between ***40*** and ***60 [Hz]*** the mass lines are much more comparable than between ***10*** and ***60 [Hz]***.

It proves that measuring the hub in the low frequency region is a difficult job to do and indeed some tools are needed to check the measurement data.

So with the two models of blade and two models of the hub, the four possible coupling variants (combinations) are made:

1. regenerated blade-lumped hub (RBL)

2. regenerated blade-full hub (RBF)

3. measured blade-lumped hub (MBL)

4. measured blade-full hub (MBF)

The assembly is done in the local coordinates of the hub joint which coincide with the global coordinates of the blade. After validation it turns out that:

- *RBL* prediction is inaccurate and poor both in low and high frequency region
- *RBF* is slightly better but still isn't accurate and don't predict the reality
- *MBL* estimates the lower frequency region very accurate but at the higher region the prediction is less accurate
- *MBF* produce reliable results but prediction at the lower region is not good as *MBL* however at the higher region the prediction improves

Looking at the coupling results one may conclude:

- the regenerated blade model doesn't describe the blade reasonable and is not feasible which can be caused by; close modes, damping which is distributed in a non proportional way, the absence of proper lower and higher residual terms, too complex higher modes which not are not easily identifiable
- using the full hub model will improve the high frequency region

The MBL and MBF assemblies are further studied, evaluated and the modes are identified. Up to ***185 [Hz]***, MBL has ***9*** modes and MBF ***10***. They can be divided into five groups of modes; the first group is associated with the first bending mode of the blade as if it is clammed at its interface. The second and the third group are related to the second and third bending mode of the blade respectively. The fourth group is more complex and shows both third bending and torsion simultaneously. The fifth group is associated with the first blade torsion mode.

From the identified modes some have a very low modal damping which is maybe caused by damping in the joint which is not correctly included in the blade model. The reason could be the damping mechanism in the joint which varies due to the hub mass.

8.2 Recommendations

In principle the assembly results are promising and show that FBS in general and LM FBS in specific have the potential to couple and decouple experimental models. But there are some questions left unanswered:

- Would the blade model change if a much heavier fixture was used?
- Were the results still the same if all three blades were modeled and used in the assembly?
- Could the lumped hub model be augmented with elastic modes of the hub?

Without doubt the other substructures of the test bed needed to be modeled and the complete system can be assembled. By implications the following can be mentioned which may help during the modeling process:

- in general LM FBS coupling/decoupling formulation produce reliable prediction if the data are relatively noise-free and a set of consistent and accurate data are used
- experimental models should be constructed from a minimum set of data
- the measurement boundary condition should be comparable to that of the operational condition
- preferably use a fixture which resembles the adjacent substructure mass
- if needed, perform the assembly first in the local coordinates and then transform the results into global directions

Bibliography

[1] D. de Klerk, D. J. Rixen and S. N. Voormeeren, General Framework for Dynamic Substructuring: History, Review, and Classification of Techniques, AIAA JOURNAL, Vol. 46, No. 5, May 2008, http://dx.doi.org/10.2514/1.33274

[2] Dennis de Klerk, Daniel J. Rixen and Jasper de Jong, The Frequency Based Substructuring (FBS) Method reformulated according to the Dual Domain Decomposition method, Proceedings of the 15th International Modal Analysis Conference, Society for Experimental Mechanics, Feb. 2006.

[3] Dennis de Klerk, Dynamic Response Characterization of Complex Systems through Operational Identification and Dynamic Substructuring, An application to gear noise propagation in the automotive industry, Ph.D. Thesis, March 2009

[4] W. A. Benfield and R. F. Hruda, Vibration Analysis of Structures by Component Mode Substitution, VOL. 9, NO. 7, JULY 1971 AIAA JOURNAL.

[5] Matthew S. Allen, Randall L. Mayes, Elizabeth J. Bergman, Experimental modal substructuring to couple and uncouple substructures with flexible fixtures and multi-point connections, Journal of Sound and Vibration, Volume 329, Issue 23, http://dx.doi.org/10.1016/j.jsv.2010.06.007

[6] S.N. Voormeeren, D. J. Rixen, A family of substructure decoupling techniques based on a dual assembly approach, Mechanical Systems and Signal Processing, Volume 27, http://dx.doi.org/10.1016/j.ymssp.2011.07.028

[7] R.A.B. Almeida, A.P.V. Urgueira, N.M.M. Maia, Identification of rigid body properties from vibration measurements, Journal of Sound and Vibration 299 (2007), pages 884–899.

[8] Jens Wittenburg, Dynamics of Systems of Rigid Bodies, B.G. Teubner, Stuttgart 1977.

[9] Carsten Schedlinski, A survey of current Inertia Parameter Identification methods, Mechanical Systems and Signal Processing (2001) 15(1), pages 189-211, http://dx.doi.org/1006/mssp.2000.1345

[10] Anthnio P. V. Urgueira, On the Rigid Body Properties Estimation from Modal Testing, Proceeding of 13th International Modal Analysis Conference, pages 1479-1483.

[11] Hyuk Lee, Yoon-Bok Lee, Youn-Sik park, Response and excitation points selection for accurate rigid body inertia properties identification, Mechanical Systems and Signal Processing (1999) 13(4), pages 571-592.

[12] S.N. Voormeeren, D. de Klerk, D.J. Rixen, Uncertainty quantification in experimental frequency based substructuring Mechanical Systems and Signal Processing 24 (2010), Pages 106–118.

[13] Daniel J. Rixen How measurement inaccuracies induce spurious peaks in Frequency Based Substructuring, International Modal Analysis Conference, IMAC-XXVI, 2008.

[14] Randy L. Mayes, Wind Turbine Experimental Dynamic Substructure Development, Proceedings of the SEM IMAC XXX Conference, 2012.

[15] Julie Harvie, Peter Avitabile, Comparison of Some Wind Turbine Blade Tests in Various Configurations, Proceedings of the SEM IMAC XXX Conference

[16] Randy L. Mayes, Assembly instructions for Ampair 600 Wind Turbine Test Bed

[17] Randall J. Allemang, The Modal Assurance Criterion –Twenty Years of Use and Abuse. Proceedings of IMAC 20, the International Modal Analysis Conference, Los Angeles, CA, U.S.A. (2002), pp. 397–405

[18] Allyn W.Phillips, Randall J. Allemang, Wiliam A.Fladung, The Complex Mode Indicator Function (CMIF) as a Parameter Estimation Method, Proceeding of the IMAC-XVI, 1998.

[19] D. J. Ewins, Modal Testing: Theory, Practice and Application, Second Edition, Research Studies Press LTD, England, 2000.

[20] Gene H. Golub, Charles F. Van Loan, Matrix computations, The Johns Hopkins University Press, Baltimore (1996) Third Edition.

[21] Alain Girard and Nicolas Roy, Structural Dynamics in Industry, ISTE Ltd and John Wiley & sons, Inc

Appendix A

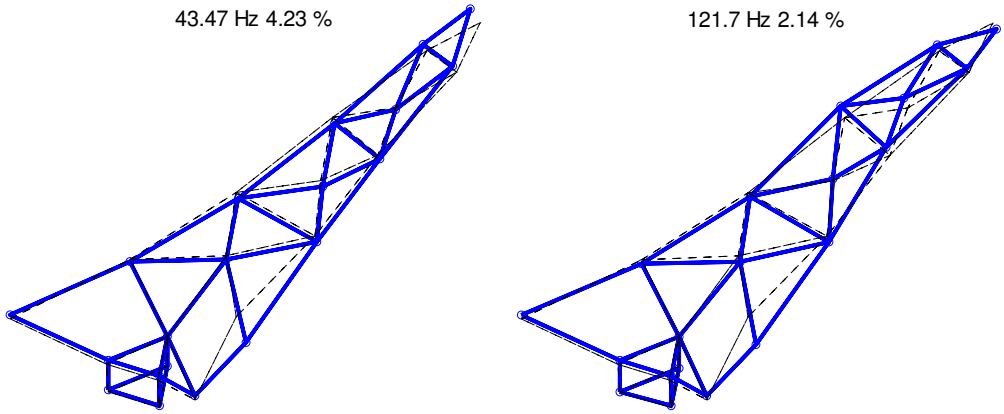

Figure A-1; 1st and 2nd blade mode

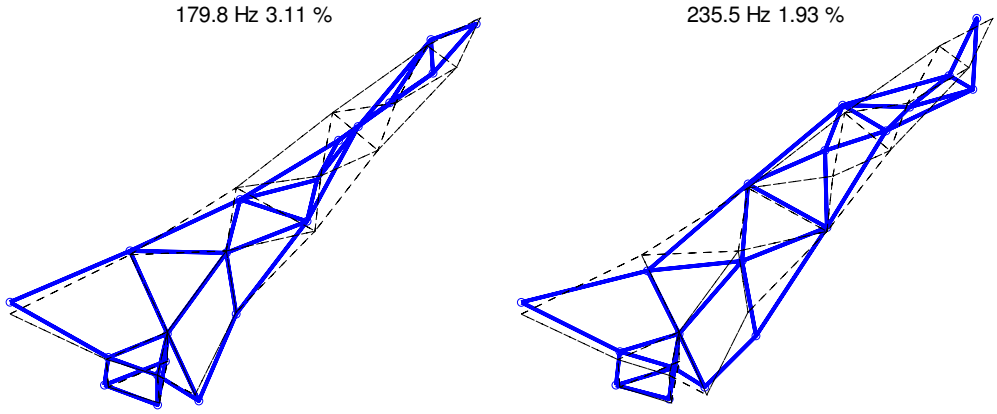

Figure A-2; 3rd and 4th blade mode

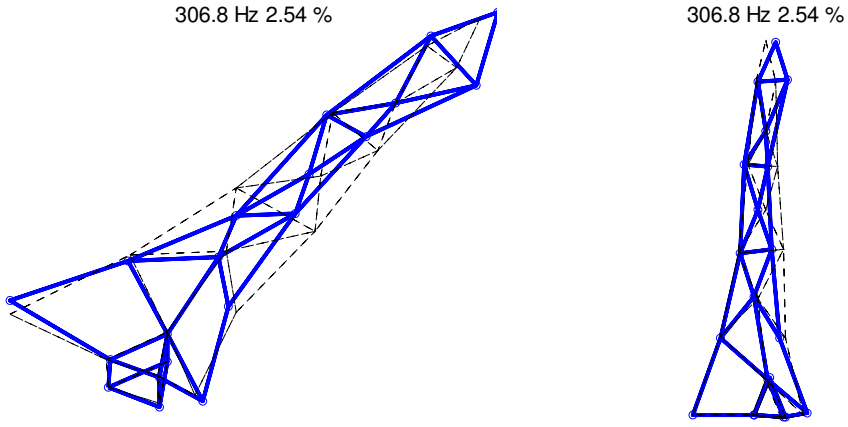

Figure A-3; 5th blade mode inclusive the side view

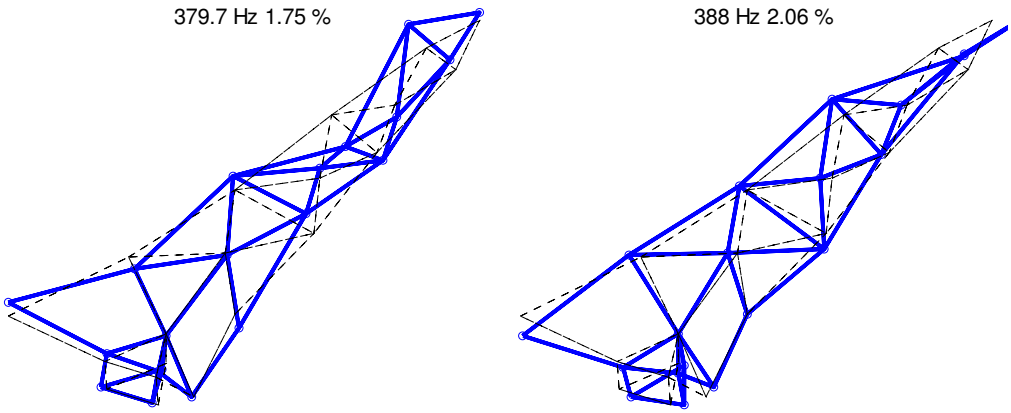

Figure A-4; 6th and 7th blade mode

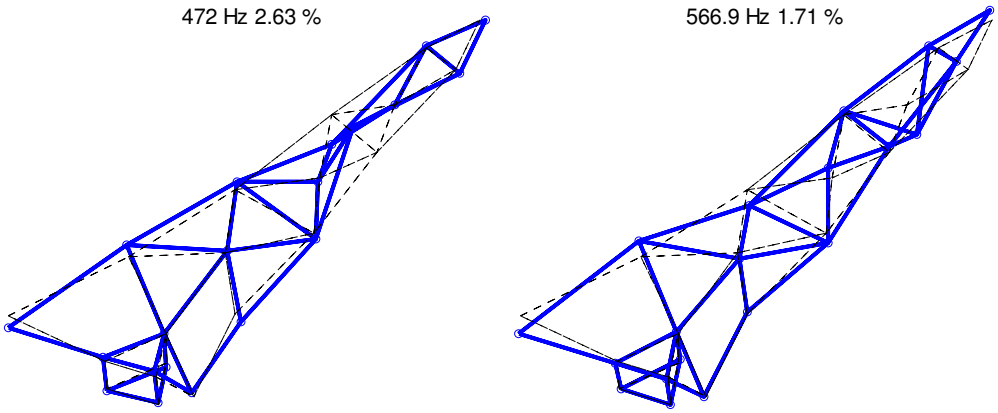

Figure A-5; 8th and 9th blade mode

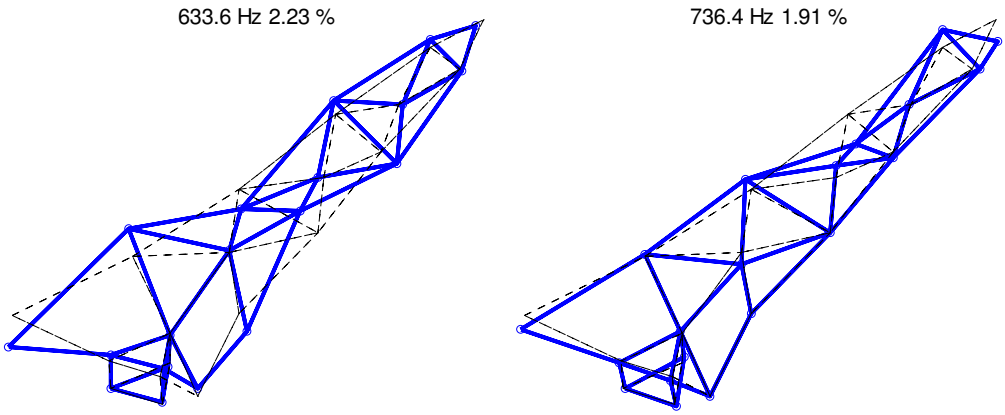

Figure A-6; 10th an 11th blade mode

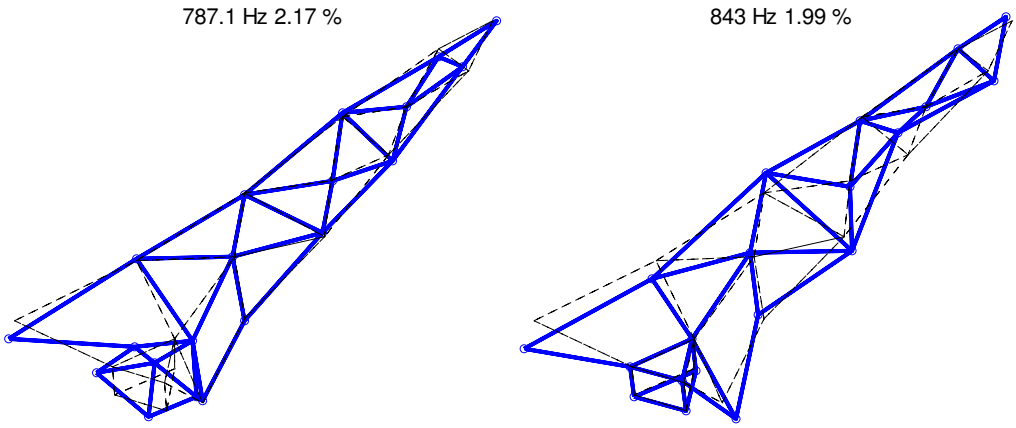

Figure A-7; 12th and 13th blade mode

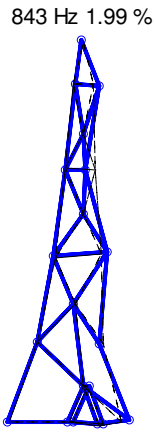

Figure A-8; Side view of the 13th blade mode

Appendix B

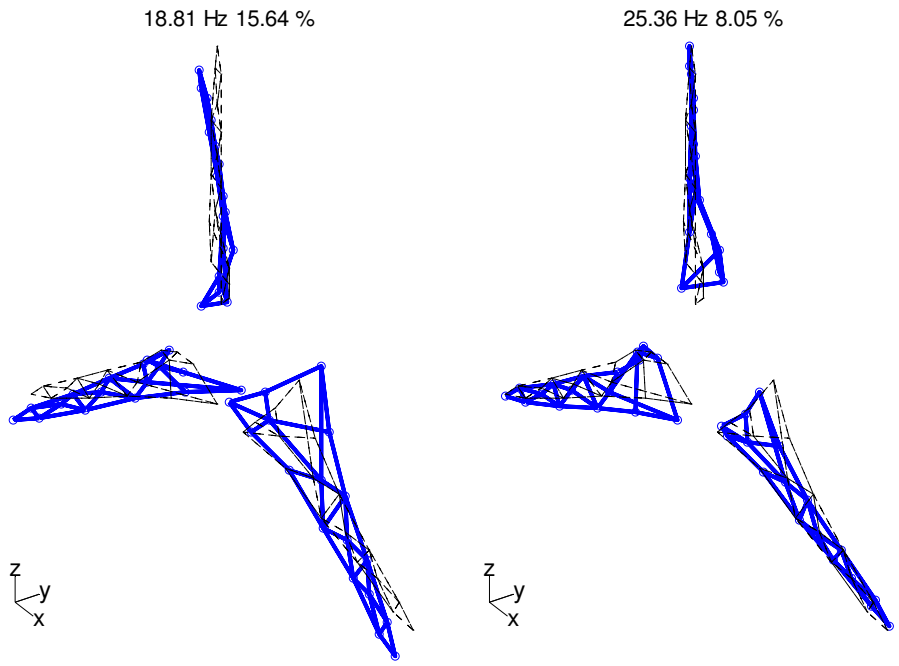

Figure B-1; 1st and 2nd MBF Assembly mode

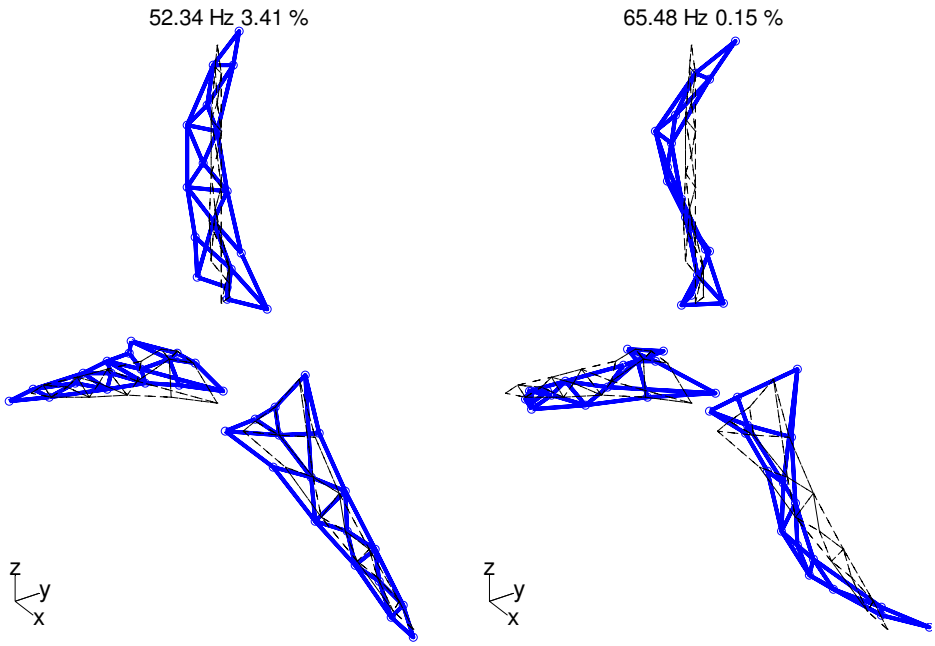

Figure B-2; 3rd and 4th MBF Assembly mode

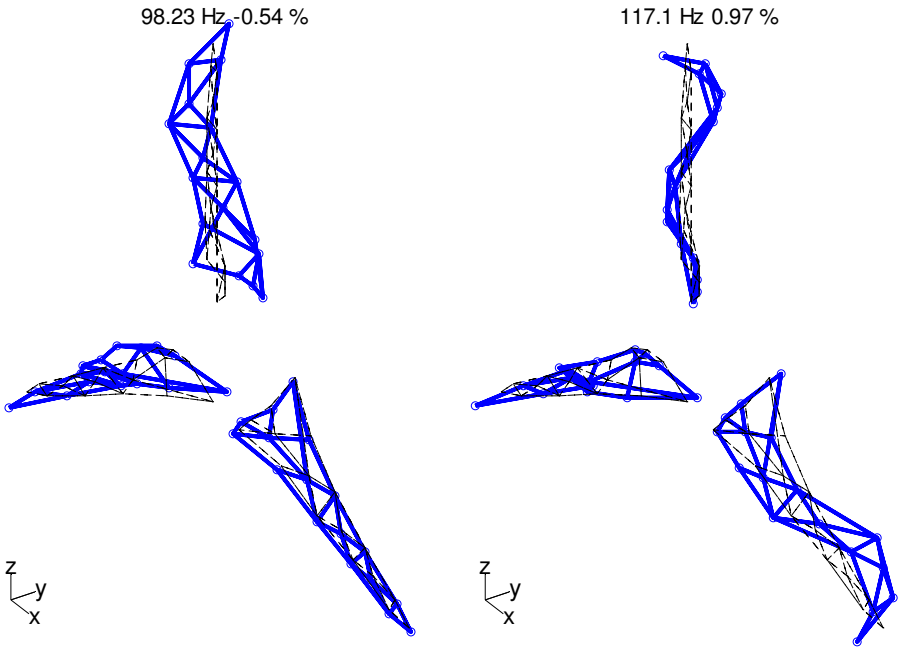

Figure B-3; 5th and 6th MBF Assembly mode

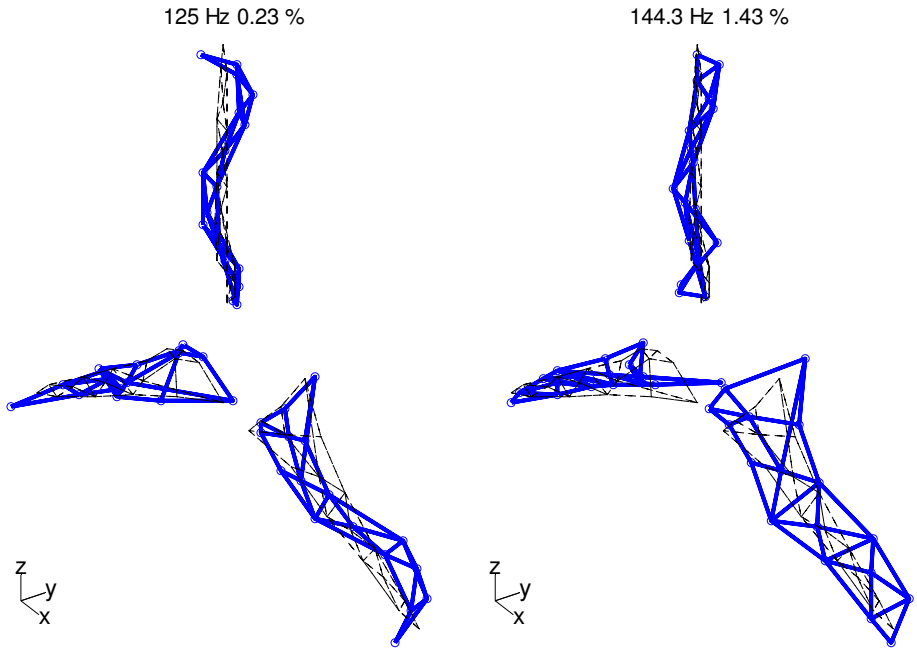

Figure B-4; 7th and 8th MBF Assembly mode

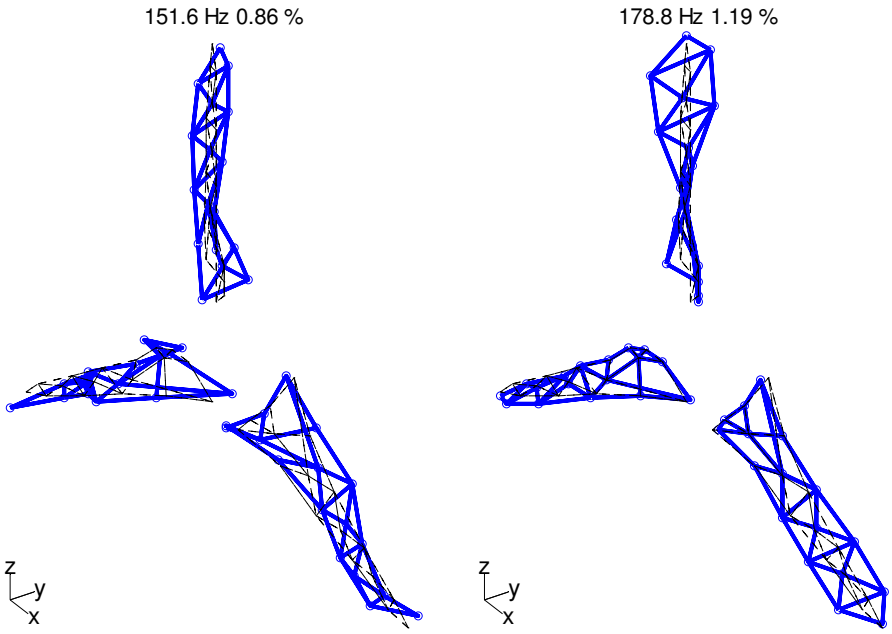

Figure B-5; 9th and 10th MBF Assembly mode

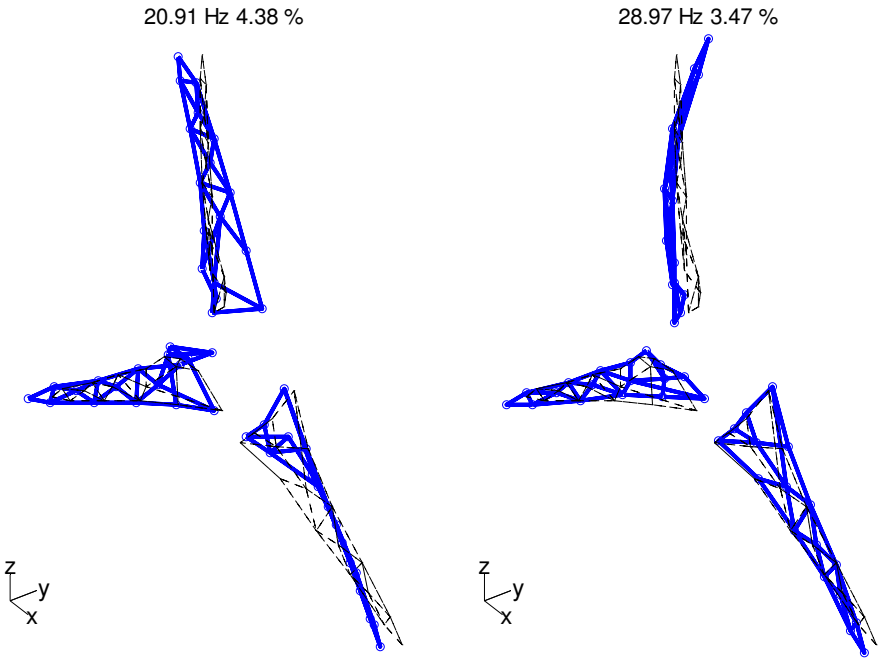

Figure B-6; 1st and 2nd MBL Assembly mode

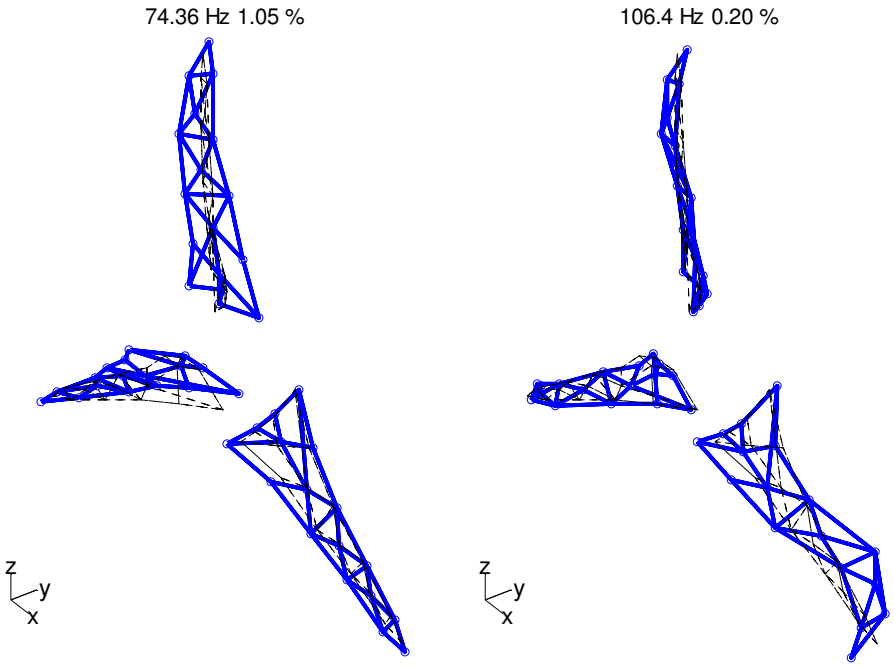

Figure B-7; 4th and 5th MBL Assembly mode

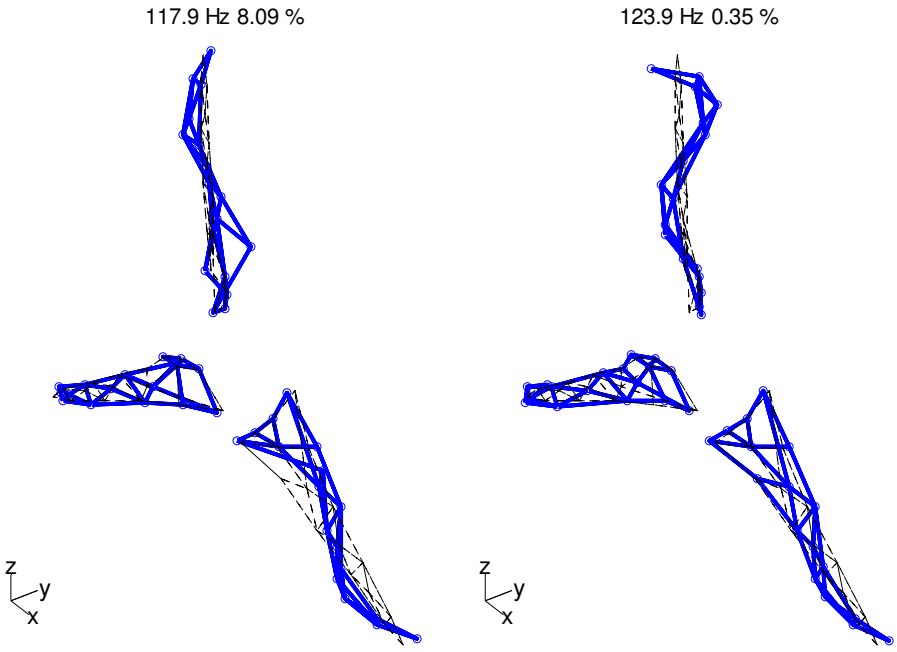

Figure B-8; 6th and 7th MBL Assembly mode

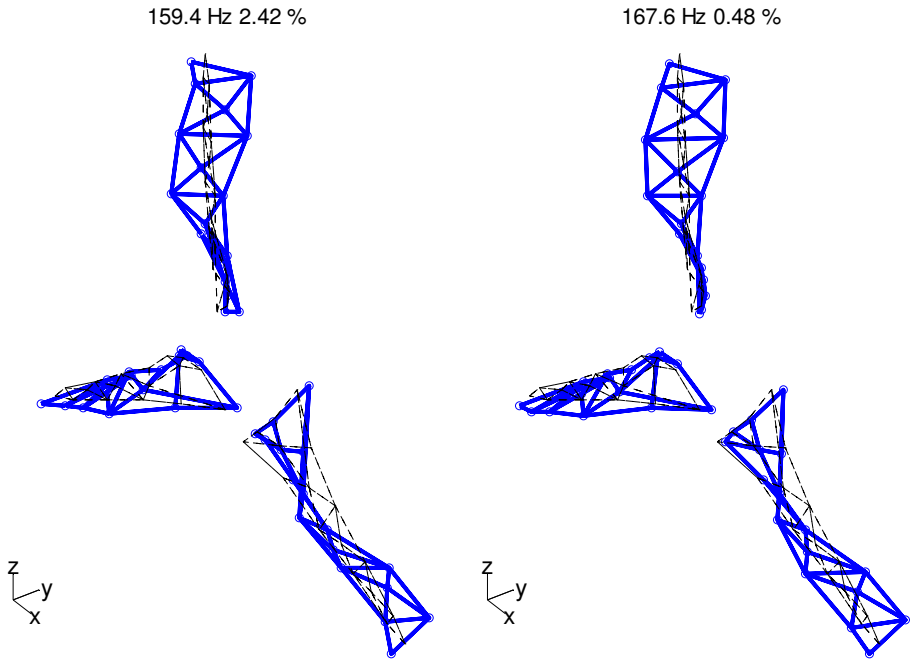

Figure B-9; 8th and 9th MBL Assembly mode

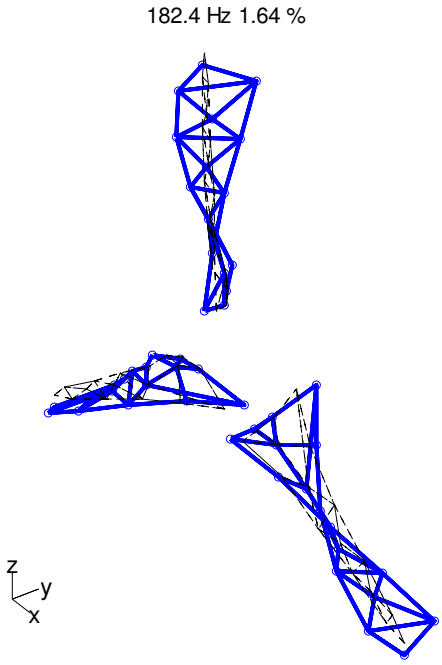

Figure B-10; 10th MBL Assembly mode

Appendix C

The resin mixture to fill the pitch mechanism cavity with is formulated from the materials given in Table C-1 on the weight basis. The minimum batch size is ***105 [g]*** and maximum is ***1155 [g]***.[1]

Material	Parts by weight
EPON 828 Epoxy	75 [g]
Glass Microspheres (GMB)	21 [g]
DEA (Diethanolamine)	9 [g]

Table C-1; Resin mixture materials

THE RESIN AND CURING COMPONENTS MAY BE TOXIC. THEREFORE, ADEQUATE VENTILATION SHOULD BE PROVIDED IN THE HANDLING OF THESE COMPONENTS TO PREVENT UNDUE EXPOSURE TO VAPORS. INGESTION OR SKIN CONTACT WITH THESE MATERIALS SHOULD BE AVOIDED. SHOULD ACCIDENTAL SKIN CONTACT OCCUR, THE EXPOSED AREAS SHOULD BE WASHED IMMEDIATELY WITH SOAP AND WATER

Degrease the hub cavity, the pitch mechanism, the locking shaft and the disk with acetone or/and alcohol.

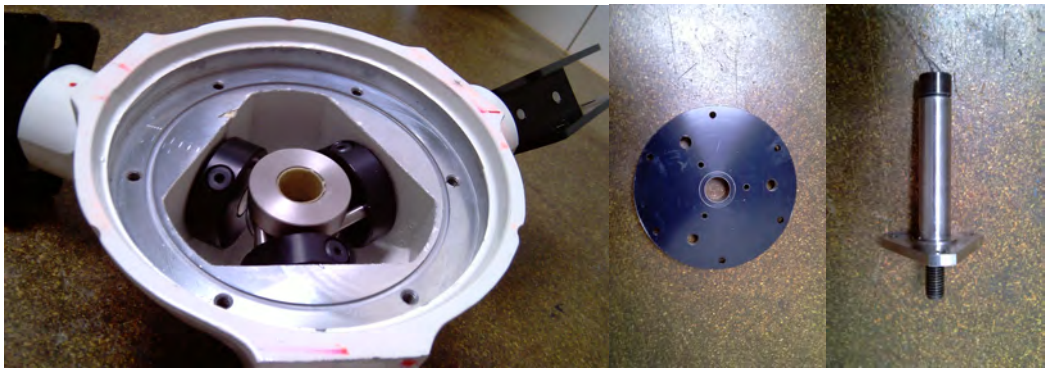

Table C-2; Hub assembly components to be degreased

Weigh the required amounts of EPON 828 and GMB into a suitable container. Preheat the 828 resin, the DEA, the GMB and the assembled hub at ***71°C*** for at least ***2*** hours.[2] To ensure GMB is DRY and free flowing, dry for ***6*** hours minimum. If necessary, use aluminum foil as a cover to keep the filler from "blowing" around in the oven.

[1] This formulation is provided by Howard W. Arris from Sandia National Laboratories.

[2] GMB is the filler and the DEA is hardener.

If you do not have heated vacuum chambers, use a large heat sink such as a metal block heated to ***71°C*** and place mixing container on this when mixing, degassing etc. to maintain material temperatures.

Table C-3; Mixture resin materials and the hub in the oven

Add the GMB to EPON and mix mechanically until the mixture is uniform and then add the DEA. Make sure that the material on the bottom and corners of the mixing container are mixed in. we have used a magnetic stirrer with a heat sink to maintain temperature during mixing.

Table C-4; Mixing the resin materials on the magnetic stirrer

Put the heat sink and resin mixture in the vacuum chamber and form vacuum very slowly down to ***0.004 bar***. **Note!** The container should be large enough to accommodate the foam rise of the resin during evacuation; this is typically ***4-5*** times the volume of mixture. De-air resin mixture for ***1-3*** minutes after the foam rise.[1]

[1] At this point verify that the material has exothermed to ***>82°C***, if it has not place the batch back into the ***71°C*** oven, until the exotherm exceeds ***82°C***. This step is important, the DEA is not immediately soluble in the epoxy, but becomes soluble during the initial exothermic reaction. Upon addition of the DEA, the material is cloudy, as the exothermic reaction progresses the formulation will become clear.

Table C-5; Resin mixture in the vacuum chamber to be degassed

Break the vacuum to atmosphere very slowly and then the chamber can be opened. **Note!** The time from addition of DEA to breaking the vacuum to atmosphere should be accomplished within 30 minutes. The resin can be poured in to the hub. At the time of pouring the hub should be at a minimum temperature of $82°C$. The part shall then be cured at a temperature of $71°C$ for 16 hours minimum.

Table C-6; Pouring the resin inside the hub cavity

Table C-7; Curing the poured resin inside oven